The efficiency of maltodextrin and porous silicon nanoparticles for the *in vitro* and *in vivo* stabilization of tyrosine hydroxylase

Fredrik Gullaksen Johannessen

This thesis is submitted in partial fulfillment of the requirements for the degree of Master of Science as part of the work during the Master's programme in Nanoscience.

Department of biomedicine, University of Bergen

June 2016

Abstract

Parkinson's disease is a severe neurodegenerative disease, which causes deterioration of the dopaminergic neurons of the substantia nigra. Lack of dopamine causes motor function problems and cognitive decline. Due to unwanted side effects resulting from the traditional treatment of the disease by L-DOPA, the use of formulations of tyrosine hydroxylase (TH), the rate limiting enzyme in the biosynthesis of dopamine, could yield an effective treatment with less side effects. This is due to the high level of regulation TH is subject to compared to L-DOPA. To further increase delivery to the target site, the use of nanoparticles as nanocarriers can be used. Maltodextrin nanoparticles (MDNPs) and porous silicon nanoparticles (pSiNPs) were investigated to this respect.

DLS was used as a simple method of confirming or debunking loading of NPs, since TH and each NP originated distinct size peaks (approximately 13 nm for TH, 90 nm for MDNPs and 120 nm for pSiNPs) when measured. Loading was easily confirmed for the TH:MDNPs complex, but not for the pSiNPs, where DLS measurement in the buffer (50 mM HEPES, pH 6, 50 mM NaCl) and concentrations (0.1 mg/ml in 1:10 000 pSiNPs) that no longer showed free TH, but we could not distinguish between pSiNPs peaks and aggregates of TH. A Thioflavin-T assay was performed in order to find out whether the presence of pSiNPs promoted the aggregation of TH, or if it hindered it. Through these experiments it became clear that the pH of the buffer was the most significant factor associated to aggregation, but that this effect could be avoided by altering the pH of the complex from pH 6 to pH 7. Since MDNPs loading was the most successful, the stability of TH:MDNPs was studied *in vitro* by using DLS to look at the diameter of the average size of particles in the sample solution over time and at different temperatures. In both cases it was found that a 1:1 w/w ratio of TH:MDNPs would prevent aggregation, and also that a 2:1 w/w ratio TH:MDNP would at least delay the effects of aggregation.

Activity measurements also revealed that TH retained activity in both complexes, but more so in MDNPs. *In vivo* injection of TH:MDNPs was performed in order to find out if the complex could be taken up by brain cells. Fluorescent tags were used, and TH:MDNP-Atto488 and TH-Alexa568:MDNP was injected, and was located in tissues near the injection site using fluorescence microscopy. Further investigation using confocal microscopy showed that the complexes were very likely to have been taken up by the cells.

Abstrakt

Parkinsons sykdom er en alvorlig nevrodegenerativ sykdom, noe som fører til at de dopaminergiske nevrecellene i substantia nigra. Mangel på dopamin fører til motorikkproblemer og kognitiv svikt. På grunn av uønskede bivirkninger som følge av den tradisjonelle behandlingen av sykdommen kan bruk av tyrosin hydroksylase (TH), det hastighetsbegrensende enzymet i biosyntesen av dopamin, gi en effektiv behandling med mindre bivirkninger. Dette er på grunn av det høye nivået av regulering TH er underlagt i forhold til L-DOPA. For ytterligere å øke levering til målstedet kan nanopartikler (NPs) benyttes som nanobærere. Maltodekstrin nanopartikler (MDNPs) og porøst silisium nanopartikler (pSiNPs) ble undersøkt for slik bruk.

DLS ble brukt som en enkel metode for å bekrefte eller avkrefte lasting av NPs, siden TH og de ulike NPs stod for forskjellige topper på grunn av deres størrelse målt i DLS (ca. 13 nm for TH, 90 nm for MDNPs og 120 nm for pSiNPs). Lastingen ble lett bekreftet for TH:MDNP komplekset, men ikke for pSiNPs, hvor DLS måling i den bufferen (50 mM HEPES, 50 mM NaCl, pH 6) og konsentrasjonen (0,1 mg / ml i 1:10 000 pSiNPs) som ikke lenger viste fri THmen hvor vi ikke kunne skille pSiNPs topper fra TH aggregater som ble dannet. En Thioflavin-T analyse ble utført for å finne ut hvorvidt nærværet av pSiNPs fremmet aggregering av TH, eller hvis det hindret den. Gjennom disse forsøkene ble det klart at pH-verdien i bufferen var den viktigste faktor når det kom til aggregering, men at denne effekten kunne unngås ved å endre pH-verdien av komplekset fra pH 6 til pH 7. Siden MDNPs lastingen var den mest vellykkede, ble stabilitet i TH:MDNP undersøkt *in vitro* ved hjelp av DLS for å se på diameteren til den gjennomsnittlige størrelse av partikler i prøveløsningen over tid og ved forskjellige temperaturer. I begge tilfeller ble det funnet at en 1:1 vekt/vekt-forhold på TH:MDNP ville hindre aggregering, og også at en 2:1 vekt/vekt-forhold TH:MDNP ville i det minste forsinke virkningene av aggregering.

Aktivitetsmålinger avslørte også at TH beholdt aktivitet i begge komplekser, men i større grad i TH:MDNP. *In vivo* injeksjonen av TH:MDNP ble også utført for å finne ut om komplekset kan bli tatt opp av hjerneceller. Fluorescente fargestoff ble benyttet, og TH:MDNP-Atto488 og TH-Alexa568:MDNP ble injisert, og lå i vev nær injeksjonsstedet, funnet ved hjelp av fluorescens mikroskopi. Videre undersøkelser ved hjelp konfokalmikroskopi viste at kompleksene svært sannsynlig hadde blitt tatt opp av cellene.

Contents

Acknowledgements

Firstly, I would like to thank my supervisors Maria Teresa Bezem, Lars Herfindal and Aurora Martinez, who went above and beyond, and for their aid and mentorship I am truly grateful. Whenever I needed help they were there to lend a helping hand and sound advice.

I thank Anne Baumann for help with the Thioflavin-T assay training and set-up and for the liposomes used as positive control in this experiment. I thank Ali Javier Sepulveda Muñoz and Khanh Kim Dao for purification of the fusion protein, Maria Teresa Bezem and Marte Innselset Flydal for cleavage of this fusion protein, all aiding to provide me with purified TH. I also thank Mihaela Roxana Cimpan and all the good people at the Department for Clinical Dentistry for introducing me to cell culture and toxicity studies which will undoubtedly prove incredibly useful in the project's future.

A deep heartfelt thanks to the Biorecognition group at the Department for Biomedicine is also in order. Their help and guidance throughout this master's project has been truly wonderful.

Thanks also to my good friends, and fellow masterstudents Edvin Tang Gundersen and Ørjan Handegaard for good discussions and helpful advice. The fluorescence and confocal imaging was performed at the Molecular Imaging Center (MIC) and was thus supported by the Department of Biomedicine and the Faculty of Medicine and Dentistry, at the University of Bergen, and its partners.

Abbreviations

BBB	Blood-brain barrier
BH_4	Tetrahydrobiopterin
DDC	Dopa decarboxylase
DLS	Dynamic light scattering
DPPG	Dipalmitoylphosphatidylglycerol
ERT	Enzyme replacement therapy
HPLC	High performance liquid chromatography
L-DOPA	L-3,4-dihydroxyphenylalanine
MBP	Maltose binding protein
MDNPs	Maltodextrin nanoparticles
NPs	Nanoparticles
NCs	Nanocarriers
PD	Parkinson's disease
pSiNPs	Porous silicon nanoparticles
TH	Tyrosine hydroxylase
Th-T	Thioflavin-T
WGA	Wheat germ agglutinin

Well-known abbreviations frequently used in chemistry or molecular biology are not included.

1 Introduction

1.1 Parkinson's Disease

Parkinson's disease (PD) is a progressive neurodegenerative disorder. This means that it is characterized by an increasing loss of neurons mainly consisting of the dopaminergic neurons in a part of the basal ganglia called the substantia nigra [1]. Dopaminergic neurons are neurons that use dopamine as their main neurotransmitter. A neurotransmitter is a signaling molecule released into the synapse, the axonal area between two neurons. This is in order to transfer the electric signal from the axon potential from the presynaptic neuron to a chemical signal that can be received by the next neuron in the signaling circuit, the postsynaptic neuron. The neurons that degenerate in PD participate in the signaling needed for motor skills, hormone release and reward-motivated behavior. The most typical symptom of PD is therefore the loss of motor function and uncontrollable tremor, but in addition to these motor impairments. PD patients could also be subject to several psychological symptoms, such as depression, apathy, sleep disturbance and a general cognitive decline. The cause of the neurodegeneration observed in PD is still unknown, but the presence of intracellular inclusions of α-synuclein has been linked to the progression of the disease [2]. The available treatments for PD are usually symptomatic, meaning they give relief for the symptoms that comes with PD, and not the underlying cause. These treatments often focus on increasing dopamine levels or enhancing the effect of the dopamine signaling. There also exist other neurological disorders characterized by low levels of dopamine, like parkinsonisms and dystonias, as well as tyrosine hydroxylase deficiency (THD), caused by mutations in TH. All these disorders have symptoms similar to those for PD, but are usually not neurodegenerative, i.e. TH function is affected but neuronal death is not manifested [3, 4].

1.2 Dopamine in neurotransmission

1.2.1 Dopamine biosynthesis

Dopamine, noradrenaline and adrenaline are a group of neurotransmitters and hormones called the catecholamines. These compounds are characterized by a benzene ring with two adjacent hydroxyl groups and an amine group. The biosynthesis of the catecholamines (Figure 1).

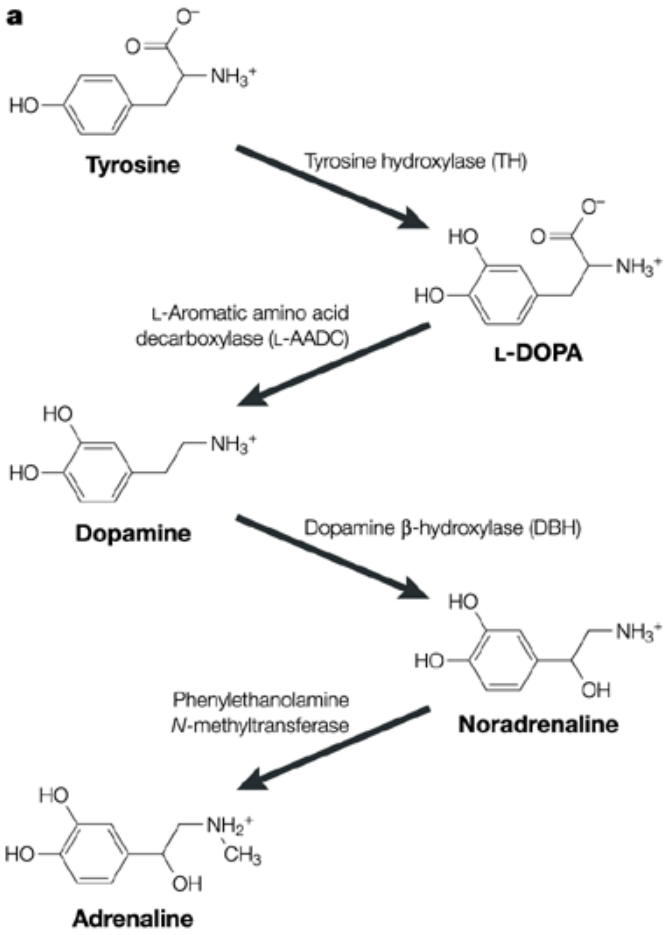

Figure 1: The catecholamine biosynthesis. *The first and rate-limiting step is the reaction transforming L-Tyrosine to L-DOPA, catalyzed by the enzyme tyrosine hydroxylase. L-DOPA is further converted into dopamine from which the other catecholamines are synthesized. The enzymes catalyzing the different steps are also shown. Figure is taken from [7].*

1.2.2 Dopamine release

Neurons that utilize catecholamines as neurotransmitters are referred to as monoaminergic neurons or more specifically dopaminergic, noradrenergic or adrenergic neurons depending on which neurotransmitter they mainly use. The catecholamines are stored in synaptic vesicles, and upon signaling, exocytosis of the vesicles' contents occur. When an action potential reaches the synapse of a monoaminergic neuron, the influx of Ca^{2+} causes the vesicles to merge with the synaptic membrane, releasing their contents into the synaptic space by exocytosis[8]. The vesicles are quickly recycled by endocytosis, whereas dopamine binds to receptors on the postsynaptic side of the synapse and is then either recycled or degraded.

1.2.3 Dopamine storage

The catecholamines storage in vesicles is energy dependent and mediated by the transport protein called vesicular monoamine transporter located in the vesicular membrane. The energy that is required for this transport is provided by vacuolar-type H^+-adenosine-triphosphatase (ATPase) coupled to vesicular monoamine transporter 2 (VMAT2). The first two steps of the catecholamine biosynthesis pathway happen in the cytosol and thus dopamine is synthesized in the cytosol, but then quickly stored in vesicles, through VMAT2. Vesicular dopamine can, depending on the type of neuron, be used as a neurotransmitter or be further converted into noradrenaline or adrenaline which happens inside the vesicles.[8]

1.2.4 Dopamine signaling

Catecholamine receptors are G protein-coupled receptors and there are five dopamine receptors that are categorized into two groups: the D_1-like receptors and D_2-like receptors. The D_1-like receptors are coupled to adenylyl cyclase via a stimulating GTP-binding protein, and D_2-like receptors inhibit adenylyl cyclase . Should the sum of signal molecules on the postsynaptic side of the synapse add up to activation of AC, then cAMP is formed which in turn affects Protein Kinase A. This leads to a signaling cascade in the postsynaptic neuron.[8]

1.3 Tyrosine hydroxylase (TH)

1.3.1 Catalysis performed by TH

In 1964, Nagatsu et. al. [6] described the role of tyrosine hydroxylase (TH) as the enzyme catalyzing the conversion of L-tyrosine to L-DOPA which is the rate-limiting step in the biosynthesis of catecholamines and therefore subject to many levels of regulation. TH is a homotetramer, meaning that it consists of four identical monomers containing a catalytic, regulatory and oligomerization domain. In order to catalyze the reaction TH needs requires tetrahydrobiopterin (BH_4) and molecular oxygen as co-substrates and Fe^{2+} in the active site of each catalytic domain. The importance of TH can be illustrated with the study of TH knock-out mice which showed that mice without TH were not viable [9]. In humans, the gene coding for TH is built up of 14 exons, which gives rise to four different isoforms of human TH due to alternative RNA splicing [10]. All isoforms are found in the human brain [11] and the adrenal medulla [12]. Figure 2 shows the crystal structure of the catalytic and oligomerization domains of TH.

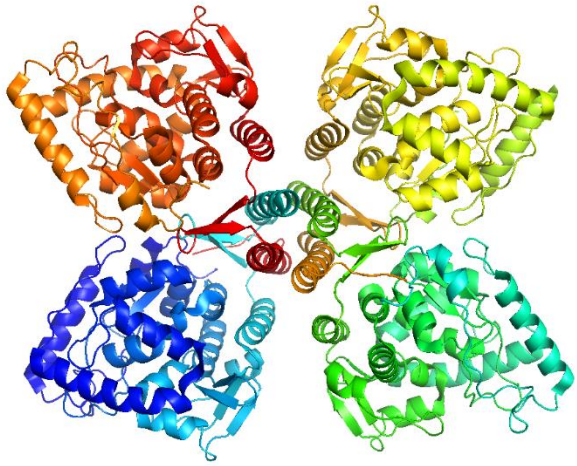

Figure 2: The crystal structure of tetrameric human tyrosine hydroxylase catalytic and oligomerization domains *(PDB ID: 2XSN). The image is made with PyMOL v0.98.*

1.3.2 Regulation of TH

Tyrosine hydroxylase is regulated on several levels, both at transcription, mRNA levels and post-translationally. Several promoter sequences upstream of the initiation site of the *TH* gene help control transcription using various transcription factors [13]. TH is also regulated by phosphorylation, dephosphorylation, feedback inhibition by catecholamines and substrate inhibition [13]. There are four phosphorylation sites at positions 8, 19, 31 and 40 in the isoform 1 of human TH, at different Ser/Thr residues in the N-terminal of the regulatory domain of TH. Phosphorylation of these residues changes the protein stability, its affinity for binding partners and inhibitors and it can activate the enzyme.

1.3.3 Recombinant TH

The method used for the expression and purification of human TH isoform 1, hTH1, used throughout the experiments (unless otherwise stated) is described here. TH was overexpressed in *E.Coli* as a fusion protein, and hexahistidine and maltose binding protein (MBP) were the fusion partners. After lysis of the bacteria, the fusion protein is purified by affinity chromatography on amylose resin, and the tags are cleaved off by tobacco etch virus protease. The TH obtained after the subsequent gel filtration gives large amount of pure, non-aggregating, thermally stable and highly active TH with intact N-terminal and iron in its active site that can be stored in liquid nitrogen until use.[14]

1.4 Enzyme replacement therapy (ERT) with TH

1.4.1 Current treatment of Parkinson's disease (PD)

PD treatments are usually symptomatic and the most widely-used drug is L-DOPA, also called levodopa. L-DOPA, the precursor of dopamine, is taken orally, and will be converted to dopamine once it has reached the brain. This raises the levels of dopamine in the brain, counteracting lack of dopamine due to deteriorating dopaminergic neurons. This is the reason L-DOPA is the standard treatment for PD although other or additional drugs are given depending on the patient's age and functionality, and the stage of the disease progression [15]. Advantages of L-DOPA administration are the increased dopamine production resulting in higher dopamine levels in the brain and relieve the symptoms from low dopamine levels.

Problem with this treatment are the many side effects like L-DOPA induced dyskinesia, involuntary movement, as well as psychiatric disorders [16]. The development of L-DOPA induced dyskinesia has also been linked to the D_3-receptor in animals [17]. These receptors are D_2-like receptors, which are targeted in treatment. In addition to these effects there are also side effects from this treatment caused by the peripheral degradation of L-DOPA before L-DOPA reaches the brain, like nausea and the increasing concentration of levodopa required to attain the wanted effect.

Other milder drugs, often given before or together with L-DOPA, enhance the effect of the dopamine signaling. These pharmacological treatments include DDC inhibitors, like carbidopa or benserazide, that reduce the L-DOPA degradation. Furthermore, such treatments include many dopamine receptor agonists that increase the sensitivity of the D_2-like receptors for dopamine [18].

Some of the other therapies available and under development for Parkinson's patients currently include deep brain stimulation, cell transplantation and gene therapy. Deep brain stimulation is a surgery where small electro shocks are used to revive the dopaminergic neurons in the substantia nigra. This could result in improved motor function, and also some improvement of the patients psychological condition, but such a surgery includes larger risks than pharmacological drugs [19]. Because of this, deep brain stimulation is often used to relieve levodopa caused dyskinesia, meaning the DBS is used after general levodopa treatment [19].

Cell transplantation of human fetal dopaminergic neurons into the caudate nucleus or putamen has been tried and these cells have shown to become functional dopaminergic neurons in the host [20]. A challenge with this treatment is the difficulty attaining the necessary genetic purity from the cells that are to be transplanted.

Gene therapy is a treatment that utilizes nucleic acid polymers as a drug often using viral delivery, and this works by acting towards the genetic source for a disease. For PD, a recent phase ½ clinical trial using genes for dopa decarboxylase (DDC), TH and GTP cyclohydrolase which is the enzyme catalyzing the rate-limiting step in the BH_4 synthesis, showed improved motor behavior in all patients [21, 22]. It is difficult for gene therapy to attain better results than current treatment.

1.4.2 ERT as an alternative treatment for PD

Another alternative which does not require brain surgery and also avoids the side effects of increased peripheral dopamine concentration seen with L-DOPA administration, would be an enzyme replacement therapy (ERT) with TH. This therapy involves administration of TH which could increase the biosynthesis of dopamine in a natural and highly regulated manner that would be produced from L-tyrosine in dopaminergic neurons.

The method of administration will be important in order to increase dopamine levels in the brain. Intravenous injection or oral administration of TH-loaded nanocarriers (NCs) would for instance be preferable to brain surgery. The use of NCs increases TH's chances to avoid immunoclearance, crossing the blood-brain barrier (BBB) and keeping its structure and function until it has been delivered intracellularly to the brain cells. Endothelial cells linked with tight junctions build up the first component of the blood brain barrier, and is supported further by astrocytes. This membrane allows highly controlled transport into the brain. Gases, water and lipid soluble molecules can generally diffuse passively through the membrane, but specialized complexes also allows for specific transport of some other molecules as well.

There is currently several ERTs in development for several different diseases, an example of which is the use of ERT in treatment of lysosomal storage diseases. Recombinant proteins have been added to the cerebro spinal fluid for use in patients with lysosomal storage diseases[23]. Some of the diseases which fall under this category, such as sphingolipidoses, have been linked to neurodegeneration. Errors in the enzyme lysosomal hydrolase, or other enzymes used for transport of lipids, lysosomal enzymes or lysosomal membrane proteins, cause the diseases, and treatment with replacement enzymes have given some symptom relief[23, 24].

1.5 Nanocarriers (NCs)

NCs are nano-sized devices carrying either drugs, macromolecules or other molecules used for imaging or diagnosis. NCs can be solid or porous particles, liposomes, spheres, capsules etc. but are all defined by its scale and need to have a submicron size, typically between a few to a few hundred nanometers. Two different types of nanoparticles (NPs) as NCs of TH will be discussed.

1.5.1 Maltodextrin nanoparticles

Maltodextrin NPs are built up of a matrix of cross-linked maltodextrin, a branched polysaccharide of glucose resulting in positively-charged NPs. Such cationic nanoparticles can absorb large amounts of proteins and phospholipids without there being great changes to particle size [25]. Dipalmitoyl-phosphorylglycerol (DPPG) is an anionic phospholipid that can be loaded into the pores of the NPs without changing the surface charge while increasing the loading capacity even further [25].

Another factor which makes these nanoparticles good candidates to be NCs is the findings that even at 4 °C the particles will bind to the cell surface or in the paracellular areas of the BBB, temperatures of 37 °C showed that the nanoparticle will undergo transcytosis across the membrane. Filipin, a polyene antibiotic, treatment of endothelial cells allows even more NPs to be transported across a model of the BBB, although it is still unknown if the lipid loading has an effect on the crossing of the BBB. This is because the *in vitro* model of the BBB failed for this type of NPs [26]. Filipin binds to sterols in the membrane, and therefore implicates sterols in the transport. An illustration of the MDNP with TH can be seen in Figure 3.

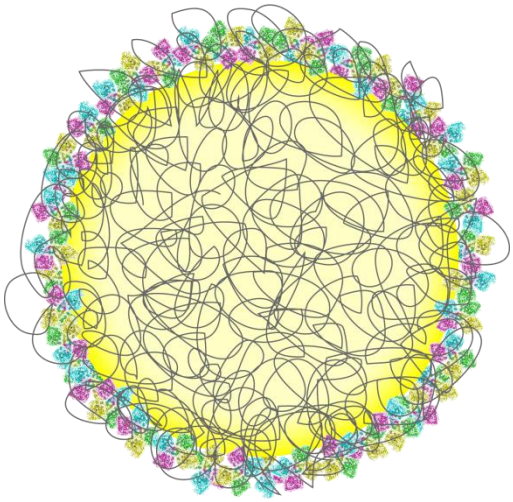

***Figure 3: The image is an illustration of a maltodextrin nanoparticle loaded with TH**. The maltodextrin matrix has the DPPG at its core (yellow), and TH is gathered in the outskirts of the illustration particle (Exactly how the TH enters into complex with MDNPs is unknown). Thanks to Helene Bustad Johannessen for this illustration.*

1.5.2 Porous Silicon Nanoparticles

The use of porous silicon NPs as NCs is potentially very beneficial, since these NPs have been found to have a relatively high capacity for loading different payloads, as well as being biocompatible and biodegradable. The nanoparticle synthesis starts with a silicon wafer, which is exposed to hydrofluoric acid, HF. Pores are etched into the wafer after a current is applied, and the pore size is dependent on the strength of this current. After the etching the wafer is sonicated. In summary, the pore size can be controlled by the voltage, and the nanoparticle size is controlled by the duration and strength of the sonication of the etched wafer [27].

Mesoporous, silicon membranes, where mesoporous signifies pore size from 2 to 50 nm, have been shown to act as nanoreactors, a complex in for protease [28], which could make the nanoparticles previously described a suitable candidate as a NC of TH. This is due to the chemical similarities between the porous silicon nanoparticles and the mesoporous silicon membrane. In Figure 4 the pSiNPs can be seen.

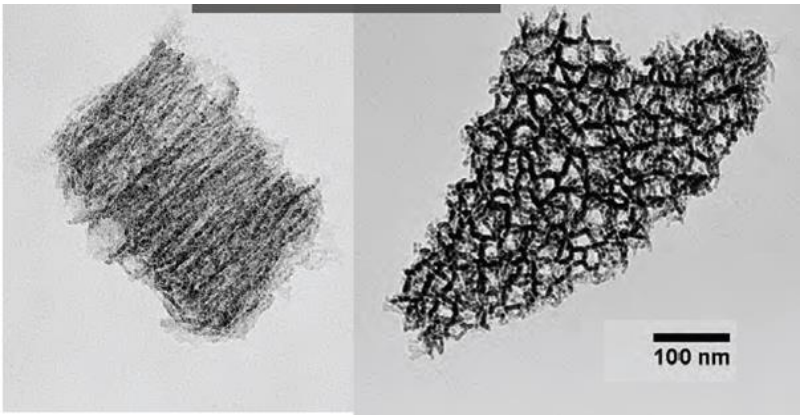

***Figure 4: Illustration of the pSiNPs used for this experiment**, courtesy of Michael J. Sailor*

1.5.3 Toxicity

In order for NCs to be a feasible alternative to ensure TH delivery in the brain it is paramount that the particles themselves are not toxic. The main component in the maltodextrin NPs are maltodextrin and DPPG which are a polysaccharide and a phospholipid. Since these are both non-toxic organic molecules by themselves it is not expected that they would themselves induce any toxic effects. However, it is still important to investigate the possible effects of the TH-NPs complex as well as potential dose dependent effects. This is

why a toxicity study is necessary. The porous silicon NPs are in aqueous media rapidly broken down to orthosilicic acid. This is the natural occurring form of silicon in biological systems and excess is excreted through urine [29].

1.6 Goal of the project

Today there is clear potential for improving treatment of low dopamine levels in PD in order to find a longer lasting treatment with less side effects than those currently available. The overall goal of this project was to get further insights on the potential for stabilization of TH *in vitro* in NPs of different composition for potential use as NCs in an ERT. and on the potential treatment is the administration of TH-loaded NPs in order to have a more regulated production of dopamine. Pursuing a new type of treatment which potentially could give the same or higher symptomatic effect as the current treatment, but without the same side effects, is favorable.

There are some challenges that need to be addressed in this regard, and the main one is related to biodistribution. In order to attain the highest efficiency of the treatment most of the TH needs to reach the brain. In order to transport TH to target the brain, NCs can be used. The NPs used to carry TH need to deliver an active enzyme to the brain. The preferred method of administration would be intravenous injection of the NP-TH complex, since this would represent a smaller intervention for the patient than full brain surgery. However, in order to enter the central nervous system (CNS), the complex will need to cross the BBB after administration, which can result in the need for further specialization of the NPs. Additional challenges are also represented by the possibility of toxicity.

1.6.1 Stabilization of TH *in vitro*

The *in vitro* experiments allow study of the loading of TH into the two types of NPs. Studying this interaction between nanoparticle and enzyme should allow optimization with regards to loading capacity, the surface properties of the NPs and TH activity and enzymatic stability.

1.6.2 Stabilization of TH *in vivo*

Stabilization studies of the NP-TH complex will be conducted *in vivo* because this allows us to investigate the biodistribution. If TH stays in the extracellular matrix or is delivered intracellularly. Furthermore, how long it takes before TH is inactive or cleared are some of the things that need to be investigated.

1.7 The approach to the project

Through this master thesis different methods were used in order to look into the questions raised in the previous section. In order to study the loading onto- and release of TH from NPs some *in vitro* experiments were carried out. In order to study the NP-TH complex the potential size effects were studied with Dynamic Light Scattering (DLS). Furthermore, it was necessary to find out if the TH can be recovered once the enzyme has entered the complex. SDS-PAGE was utilized to this respect. In order to look at biodistribution the BLK-6 mouse model was used to investigate what happens to the enzyme-nanoparticle complex in vivo. All animal experiments were carried out by proficient personnel, and approved by the appropriate board of ethics. Fluorescent probes were used to identify distribution in cryosections of NP and NP-TH injected mouse brains. Mouse brains were also homogenized and the lysate used for radioactive activity assay in order to determine activity of the enzyme. Furthermore this will be used to compare the efficiency of only the TH versus TH-NP injections on L-DOPA production in the brain over a 24 h period before the animals were euthanized. In order to also determine potential toxicity of the complex a toxicity study was performed.

2 Methods

2.1 Tyrosine hydroxylase preparation

Theoretical parameters of TH were obtained by inserting the amino acid sequence of TH (UniProt accession number P07101-3) into the web-based ProtParam Tool (ExPASy). The theoretical molar extinction coefficient ε was given to be 40715 M^{-1} cm^{-1} and a theoretical absorbance at 0.1% A was 0.732, which were then used to calculate TH's concentration in mg/ml. For the conversion to molar concentration, the molecular weight of TH was also given to be 55611.9 Da by the ProtParam Tool.

2.1.1 Expression and purification

The method used for the expression and purification of human TH isoform 1, hTH1, used throughout the experiments (unless otherwise stated) is described here. TH was overexpressed in *E. coli* BL21-CodonPlus(DE3)RIL cells using a pET-MBP-1a vector as a fusion protein. Hexahistidine and maltose binding protein were the fusion partners. After lysis of the bacteria, the fusion protein is purified by affinity chromatography on amylose resin, and the tags are cleaved off by tobacco etch virus protease.

The TH obtained after the subsequent gel filtration gives large amount of pure, non-aggregating, thermally stable and highly active TH with intact N-terminal and iron in its active site that can be stored in liquid nitrogen until use [12]. The MBP-TH fusion protein was kindly purified by Ali Javier Sepulveda Muñoz or Khanh Kim Dao (University of Bergen) from clarified cell lysate and cleaved by Maria Teresa Bezem or Marte Innselset Flydal (University of Bergen) using tobacco etch virus protease as described (Bezem et al,; in revision) and stored in liquid nitrogen.

2.1.2 Protein concentration using Nanodrop

The Nanodrop is a small volume spectrophotometer which can be used to determine the absorbance at 280 nm (A_{280}). At this wavelength, the aromatic amino acids in the protein

have an absorbance maxima, and by using the molar extinction coefficient (ε) or theoretical absorbance at 0.1% (A) the concentration (c) can be calculated by the following formula:

$$c = \frac{A_{280}}{\varepsilon} = \frac{A_{280}}{A}$$

The nanodrop method presents a strong advantage in that utilizing the A_{280} to measure the protein concentration does not require adding outside reagents that could potentially interfere with the protein solution. A_{280}, the wavelength at which ultra violet radiation is absorbed by amino acids with aromatic rings, can only be used for proteins containing such amino acids. The method is relatively quick, and does not require large amounts of protein. The method is generally not as well suited for mixtures or protein samples with add-ons.

2.1.3 Protein concentration using Direct Detect

Direct Detect is an infrared spectrometry system for analyzing biological samples on sample cards with a hydrophilic polytetrafluorethylene membrane, which is transparent in the infrared spectral region. The stretching vibration of the amide bonds in the protein absorbs infrared radiation at wavelengths in 1600-1700 cm^{-1} region. The instrument is calibrated with a known concentration of bovine serum albumin and therefore gives the protein concentration directly after buffer subtraction in mg/ml. Since this method allows for measurement of protein concentration only dependent on the always present amide bonds, Direct Detect does not have the same requirements to the content of aromatic amino acids in the protein samples which are required for Nanodrop.

2.1.4 SDS-PAGE

The SDS content in the Laemmli sample buffer in which the protein is heated, ensures the denaturation, so that the proteins run linearized through the gel and are separated according to the molecular size. This method also provides a way of identifying potential contaminants in the protein samples.

2.2 Dynamic Light Scattering (DLS)

The DLS is a method that can be used for approximating the size of particles suspended in a solution based on the scattering of light sent through the sample. Particles,

aggregates or molecules in the suspension will scatter some of the light going through the detectors, and how much, and how frequently is detected, and using Einstein Stokes, and the assumption that the particles are spherical and in Brownian motion the size can be approximated. The DLS records the rates of decay of the fluctuations due to scattering light, and the rate of this fluctuation is closely correlated to the rate of diffusion of the particle [30]. It is this relation between the DLS can be used to determine the size of nanoparticles in solution based on the Einstein-Stokes equation.

$$D = \frac{k_B T}{6\pi\eta R_H}$$

Here, the diffusion coefficient for nanoparticles in a suspension, D, is found dependent on the Boltzmann constant k_B, the temperature (T) of the solution, the viscosity of the suspension (η) and the hydrodynamic radius of the nanoparticle R_H [31].

In order to find the previously mentioned rate of decay of scattered light [30], the time correlation function is used which is the raw data presented, and is used to find the diffusion constant, and then the approximate particle size.

However, there are factors that affect the measured size distribution, which need to be taken into account. The viscosity of the sample medium, the temperature at the measurement and the refractive index of the sample medium will all affect the diffusion of the suspended particles in such a way that they need to be taken into account in the calculations, and need to be entered into the software [31]. The refractive index of the suspension is the ratio of velocity of light in vacuum by the velocity of the light in the sample solution, and the viscosity could be described as the resistance to flow of a liquid [31]. The Z-average is also a DLS term that needs to be defined which is the average particle diameter.

Especially interesting for the topic of this project was the fact that in the DLS even if concentrations of aggregates are low, their contribution to detected intensity is large. This is due to Rayleigh's law, which tells us that the scattered intensity scales with the size of the particle the light was scattered off [30].

2.3 Fluorescence

Utilizing fluorescence and fluorescent microscopy has been shown to be very advantageous in several branches of cellular and molecular biology. The methods yield relatively high resolution and due to the many different fluorophores available the method can be used to label and visualize several processes at a cellular level. [32, 33]

2.3.1 Fluorescent dyes

The method used for looking at the dispersion of our compounds (NPs) of interest in the tissue samples was detecting fluorophores conjugated to the MDNP and TH respectively. A fluorophore will be excited by light of specific wavelengths, and will in turn emit light of a longer wavelength [34].

Alexa 568, with an excitation maxima at 578, and an emission maxima at 603 was the tag used to detect TH, and Atto488 was used to detect MDNPs. Atto488 has an excitation wavelength maxima at 504 nm, and an emission maxima at 521 nm in 0.1M phosphate pH 7.0.

The complexes with the fluorescent tags were injected into the mouse brains in order for the dyes to show the potential distribution of the TH:NP complexes. A major advantage with fluorescence microscopy over traditional light microscopy is the fact that the use of fluorophores allows marking and detection of very specific targets, even at an intracellular level.

2.3.2 Thioflavin-T assay

Thioflavin-T (Th-T) is a benzothiazole dye that emits fluorescence with a maximum at 482 nm upon binding to amyloid fibrils which are the results of misfolded, or partly unfolded, proteins with exposed hydrophobic residues. More specifically, Th-T binds the cross-β structure in amyloid fibrils formed as TH aggregates [35]. Amyloid fibrils are found in amyloid deposits in the central nervous system in diseases such as Parkinson's disease or Alzheimer's disease [2]. Fluorescence monitoring of Th-T binding is typically used as an indicator of fibril formation, but can also be detected in the formation of non-fibrillar soluble oligomers that contain cross beta interactions [36, 37]. In the case of TH, a Th-T assay can provide insight

into the formation of soluble aggregates that precedes protein aggregation which would prevent loading into NPs due to the increase in size and eventually a loss of activity.

2.3.3 Fluorescence and confocal imaging

Using the Leica SP5 confocal microscope the slides prepared earlier were imaged for higher level of detail, and for the possibility of preparing Z-stacks. Confocal microscopy collects lights from small sections of a sample, which allows examination of particular focal planes [33]. Because of this confocal microscopy allows for eliminating out of focus fluorescence, which would be detected in a normal fluorescence microscope [32, 34]. This is important, because the obtained Z-stacks could, and was, used for a 3D projection of the sample. The confocal microscopy used for the imaging in this thesis was the Leica SP5, a laser scanning confocal microscope, which utilizes lasers which are swept over the field of view by a scanning mirror and directing optics. The beam is focused on a single point in the sample by an objective, and the emitted light that passes through a pinhole is collected and analyzed at the detector.[32]

2.4 TH activity

TH catalyzes the reaction that synthesizes L-DOPA from L- tyrosine (Fig. 1). The specific activity of TH can be measured by controlling the time period in which the protein is allowed to be active and determining the amount of L-DOPA produced. The latter is obtained by separation from L-Tyrosine using the High Performance Liquid Chromatography (HPLC). HPLC is a method used to separate components in a mixture, in this case L-DOPA and L-Tyrosine, by sending them through a column under high pressure (up to 350 bar). L-DOPA and L-Tyrosine are chemically very similar and the buffer concentrations were optimized so that the fluorescent signal of the HPLC elution returned to baseline between the peaks. If that had not been sufficient, it would be possible to lower the run speed, although this would yield wider peaks, which would not be as easily analyzed [38].

2.5 Mouse brain study

2.5.1 Direct injection

The purposes of these injections were to visualize distribution of protein-nanoparticle complex in the tissue, and an injection site was chosen in the cortex in the front of the brain which is an area to which many dopaminergic neurons extend their axons and there is a local need for dopamine. The NP-protein complexes were injected directly into the brain instead of potentially injecting them intravenously as this was a pilot study to see what would happen to the NPs within the brain before future studies with intravenous injection are performed.

2.5.2 Cryosectioning

Cryosectioning is a method of slicing tissue samples into thin samples in order to further investigate them using histological or microscopical methods [39]. This method was used to obtain 12 µm thick horizontal sections for further analysis [40]. One of the weaknesses with this particular method is the error of the slice thickness due to the apparatus itself, being a problem if one were to estimate the thickness of the slices post sectioning [41]. Also the thinner the sections, the easier to stain them, but the more difficult to handle as there is an increased risk of losing the section due to disassembling in washing steps.

3 Experimental Procedures

3.1 Analysis of TH

3.1.1 Preparation of TH

An aliquot of TH was, except when otherwise indicated, thawn right before each experiment, diluted to 2 mg/ml in FPLC buffer (20 mM HEPES 200 mM NaCl pH 7.0) and centrifuged for 15 min at 4 °C and 20 000 g to remove aggregates. The supernatant was kept on ice until use, and the exact protein concentration was determined using either a Nanodrop 1000 (Thermo Scientific) or Direct Detect (Merck). When using the Nanodrop, the absorbance of TH at 280 nm is measured by applying 2 µl TH in solution after sample stage cleaning and measuring buffer as blank. When using Direct Detect, the infrared absorbance is measured by applying 2 µl sample or buffer onto the membrane, and inserting the sample card (Millipore).

3.1.2 SDS-PAGE

The purity of the TH samples were verified using SDS-PAGE, 95 µl 2X Laemmli sample buffer (Bio-Rad) and 5 µl 6 M DDT was mixed, and then added to the protein samples. The volumes of sample buffer and protein sample were equal, in order to dilute the 2X sample buffer to a 1X sample buffer. Afterwards the protein-buffer mix was heated at 95 °C for 5 min, and then loaded onto a Mini-PROTEAN 10% polyacrylamide gel (Bio-Rad). 20 mA was chosen to run a single gel, and 40 mA for two gels in the same tank. Finally the gels were stained with G250 Coomassie blue (Sigma) and imaged with a ChemiDoc.

3.2 Loading of TH into NPs

3.2.1 Loading of TH into MDNPs

Samples were prepared at RT. After the concentration of the TH sample was found, and 2 mg/ml stocks were prepared in FPLC buffer, 20 mM HEPES, 200 mM NaCl, the

necessary amounts for 1:1 and 2:1 w/w ratio with MDNPs were calculated. The stock solution of MDNPs with lipid DGGP+ core was provided by our collaborator Prof. Didier Betbeder from the University of Lille 2, and was 5 mg/ml. Usually 0.5 mg/ml, 1.0 mg/ml TH was used for 0.5 mg/ml MDNP. Once the NPs and TH are mixed the loading occurs on its own in the mixture.

3.2.2. Stability of TH-loaded MDNPs

In order to determine if the TH-loaded MDNPs remained stable over time at physiological temperature, DLS measurements of two ratios of TH:MDNPs, performed at regular intervals for a period of time at 37 °C, were compared to free TH (0.5 mg/ml) and non-loaded MDNPs (0.5 mg/ml). The samples were prepared in 20 mM Hepes, 200 mM NaCl, pH 7.0 in a low volume quartz cuvette (Malvern) and contained 0.5 mg/ml TH and 0.5 mg/ml MDNPs for the 1:1 TH:MDNPs and 1 mg/ml TH and 0.5 mg/ml MDNPs for the 2:1 TH:MDNPs. The samples were immediately measured using 15 runs of 15 seconds with 10 min intervals. The experiment was repeated six times, three times per batch of TH, to account for day-to-day and batch-to-batch variations.

3.2.3 TH loading into pSiNPs

pSiNPs were a gift from Maria Teresa Bezem who had prepared them in the lab of Michael J. Sailor at the University of California, San Diego. Stocks of pSiNPs are stable in ethanol for years, but the concentration of the pSiNPs stocks is not known and all experiments are performed on dilutions of the stocks. Preliminary experiments to determine the loading capacity of pSiNPs included a dilution titrations (1:100-1:10000 pSiNPs and 1 ng – 1 mg TH) that were carried out in a range of buffer concentrations (5-50 mM Hepes, 50-200 mM NaCl, pH 7.0).

To see if loading was obtained at pH 6.0, samples of 1:5000 of pSiNPs and/or 0.2 mg/ml TH were prepared in 50 mM Hepes, 50 mM NaCl at both pH 6.0 and pH 7.0 and incubated 1.5 h on ice. The sample in pH 6.0 buffer was adjusted to pH 7.0 before size distribution was analyzed with DLS. The sample in pH 7.0 buffer acted as a dilution control, so water was added so that the sample volumes would stay the same. DLS measurements were performed in triplicates in a low volume quartz cuvette (Malvern) at room temperature using an automatic run time.

3.2.4 Thioflavin-T assay

In order to confirm probable loading of TH onto the pSiNPs observed in DLS, a Th-T assay was performed to monitor the formation of oligomers. Three samples of pSiNPs (at a 1:180 dilution from stock (Here 1:1800 were the final dilution)) were loaded with 0.56 mg/ml TH in 50 mM Hepes, 50 mM NaCl at pH 6.0 for 1.5 h and then pH was adjusted to 7.0 before samples were transferred to a black Lumox multiwell plate with clear bottoms (Sarstedt).

Three identical control samples were also loaded at pH 7.0. Other controls of only TH or only pSiNPs were also prepared, and a positive control of 0.8 mM liposomes (kind gift from Anne Baumann) with 0.56 mg/ml TH was also included.

A glass bead and Th-T was added to each well to a final concentration of 20 µM Th-T and the plate was sealed with foil (Roche) right before measuring fluorescence every 5 min for 9 h in a K2 Synergy H1 hybrid reader through well bottoms. Excitation wavelength was 440 nm, emission 482 nm, gain was set to 50 and shaking was orbital. Blanks of Th-T in buffers with or without pSiNPs gave little or no fluorescence intensity and were substracted from the respective measurements, to correct for background signal.

3.4 Activity measurements

Specific TH activity was measured after 0.1 mg/ml TH was loaded into MDNPs or pSiNPs and pre-incubated with 1 % BSA (w/v) on ice by a protocol described by Fossbakk. 5 µl aliquots of the samples were incubated for 1 min at 37 °C in 40 µl reaction master mix containing 50 µM L-Tyr and 0.1 mg/mL catalase in 40 mM Na-HEPES pH 7.0 and 10 µM Fe^{2+} freshly prepared from $(NH_4)_2Fe(SO_4)_2 \cdot 6H_2O$.

The reaction was started by adding 5 µl of BH4 to final concentrations of 200 µM. The reaction was stopped after 5 min with 50 µl stop solution containing 2 % acetic acid in ethanol (v/v) and transferred to ice. Two TH samples were run in triplicates at the same time according to the set timetable (Table 1).

Table 1: Protocol for timing of activity assay. *The reaction of two samples are measured simultaneously in triplicates by starting each reaction with an offset of 20 seconds between parallels.*

Minutes	Seconds	Action
0	0	TH1→ mix1
0	20	TH1→ mix2
0	40	TH1→ mix3
1	0	BH_4 → mix1
1	20	BH_4 → mix2
1	40	BH_4 → mix3
2	0	TH2→ mix4
2	20	TH2→ mix5
2	49	TH2→ mix6
3	0	BH_4 → mix4
3	20	BH_4 → mix5
3	40	BH_4 → mix6
6	0	STOP SOL. → mix1
6	20	STOP SOL. → mix2
6	40	STOP SOL. → mix3
8	0	STOP SOL. → mix4
8	20	STOP SOL. → mix5
8	40	STOP SOL. → mix6

The samples were subsequently frozen at -20 °C for at least 30 min and centrifuged 15 min at 4 °C and 18,000 x g, before the supernatants were analyzed HPLC using a Zorbax 300-SCX column (Agilent) using a flow of 2 ml/min and a running buffer of 5 mM CH_3COOH, 2 % 1-propanol, pH 3.50 diluted with 0-50% Milli-Q water. The amount of L-DOPA was measured with fluorescence detection as described (Haavik et al 1990) The peak area of L-DOPA in the chromatography was compared to standard samples containing either 20 µM L-DOPA + 10 µM L-Tyr, 10 µM L-DOPA + 5 µM L-Tyr or 2 µM L-DOPA + 1 µM L-Tyr.

3.5 In vivo mouse brain experiment

The *in vivo* experiments were kindly carried out by prof. Lars Herfindal, to prove the ability of MDNPs to deliver TH into brain cells in intact animals. All *in vivo* experiments were

approved Norwegian Animal Research Authority and conducted according to the European Convention for the Protection of Vertebrates Used for Scientific Purposes.

The mice were kept in cages at 4-6 mice/cage with a 12/12 light/dark cycle, and had access to standard chow and water ad libido. Before injection, the mice were anesthetized with isoflurane (3mg/min induction, 1.5mg/min maintenance dose), fixed in a stereotactic frame, and given 100 µL Temgesic (0.3 mg/ml) subcutaneous in the scalp. After one minute, the scalp was opened by a longitudinal section from between the ears to the area of the occipital bone to expose the scull.

The bregma was located, and the site of injection marked 1mm anterior and 1.5mm lateral to the right side. At this point, a hole (1mm diameter) was made by a dental drill. The meninges were perforated by a needle before the injection started. The injection was done using a 10 µL Hamilton syringe with a flat needle. This was inserted 3.5 mm down from the outer surface of the scull, and 3 µL of solution was injected over a period of 1 minute. The needle was then retracted while observing that no liquid leaked from the hole in the scull.

The scalp was next closed by three to four sutures, and the mice left to recover alone in a cage. After 24 hours, the mice were euthanized by CO_2 and the brain removed, and snap frozen in liquid nitrogen or fixed in 2% formaldehyde in PBS, pH 7.4.

3.5.1 Fixation of tissue samples

The excised brains were fixed 2% formaldehyde in PBS, pH 7.4 for 48 hours at 4 °C in the dark. Afterwards all liquid was decanted from the sample tube, and 30 % sucrose was added, and the brains left in the sucrose solution until subsidence. The brains were then transferred to small pieces of paper and frozen at 80 °C, and stored frozen until cryo-sectioning.

3.5.2 Cryo-sectioning

Tissue Tek was applied to the sample holder onto which the brain is placed with ventral side down. The brains were mounted onto a sample holder using Tissue Tek, all the time ensuring that the brain was kept frozen. Horisontal sections were made at -20°C, and the thickness was 12 µm. The sections were transferred to a water bath to spread, and then

to a glass slide. These slides were then allowed to dry in a dark environment at RT for 24 hours before frozen at -20 °C for storage.

3.6 Fluorescence microscopy

3.6.1 Sample preparation

Sections on glass slides were washed three times in PBS and mounted with 6 µl Prolong Gold with DAPI mounting medium (Life Technologies) to a coverslip. For some sections, membranes were stained with DiO or WGA before mounting. In the case of DiO, 200 µL 1 µM and 2 µM preparations of DiO were added to parafilm and the section was incubated upside down in this droplet for 5 min, and washed two more times carefully in PBS before mounting. In the case of WGA staining, sections were permeabilized as indicated, washed three times in PBS, then stained with 200 µl 5 mg/ml Alexa-568-labeled WGA and washed again three times in PBS before mounting. Mounted sections were left to harden overnight in the dark at RT before imaging.

The settings for excitation and emission for both these two dyes were optimized on several samples before saving them and using them for all the brain sections examined. Fluorescent images of the mouse brain section were taken with an AxioCam HRm camera (Zeiss) on the Axioplan 2 (Zeiss) using both the 2.5x, 10x and 20x objectives for overview images and closer looks of injection sites, as well as mapping the sections. Filters for DAPI(blue), GFP(Green) and Cy 3.5(Red) were used respectively in the fluorescence microscopy For the brain maps, after the imaging, the image files were merged in the panorama function with blend in Photoshop CS4 (Adobe).

3.6.2 Confocal microscopy

High magnification confocal images were taken of the mouse brain sections using a TCS SP5 laser scanning confocal microscope (Leica) at a working distance of 0.1 mm. A 405 nm UV laser was used to excite DAPI, a 488 nm Argon laser for Atto 488, and a 543 nm HeNe laser for Alexa-568. The laser intensity, gain, and detectors were tuned in the software to give the best picture in each case, except for cases where it was necessary to compare different slides to each other. In these circumstances the same settings were found and used for all

images. For imaging immersion oil was applied to the coverslip and placed face down onto the sample holder. The images were taken using a HCX PL APO 63x 1.4 Oil objective.

4 Results

4.1 Preparation of tyrosine hydroxylase (TH)

Recombinant TH was provided after fusion protein cleavage of his-MPB-TH with tobacco etch virus protease. The success of the cleavage and the purity of TH were assessed by SDS-PAGE, and both were found to be satisfactory, though a minor band with MBP could be observed in the TH sample analyzed (Figure 5).

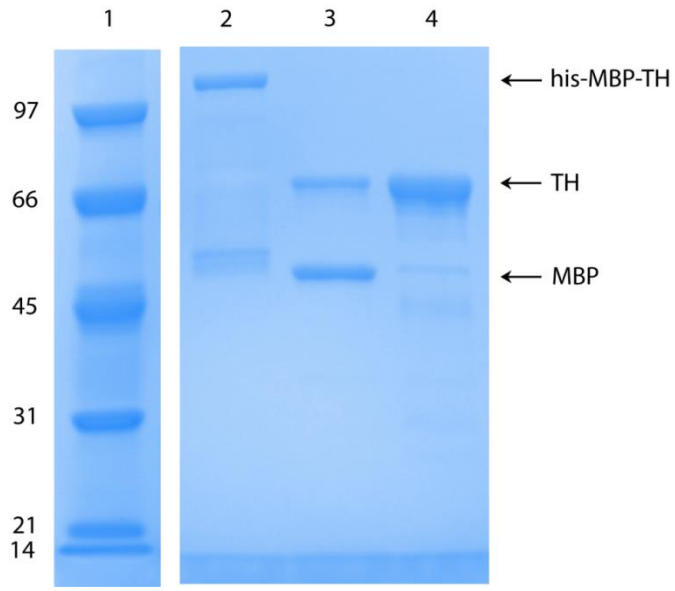

Figure 5: SDS-PAGE analysis of TH after his-MBP-TH cleavage. *Lane 1: Low molecular weight standard (BioRad). Lane 2: Uncut his-MBP-TH. Lane 3: Cut his-MBP-TH. Lane 4: Purified TH.*

4.2 Loading capacity of two nanoparticle types

4.2.1 TH loading in lipid-core maltodextrin nanoparticles (MDNPs)

Earlier titration experiments have shown that MDNPs have a large loading capacity and that up to 2 mg TH could be absorbed by 1 mg MDNPs before saturation occurs (Bezem et al.; in revision). This was verified by TH loading into the MDNPs at 1:1 and 2:1 TH:MDNPs (w/w) ratios. Subsequently, size distributions were obtained by DLS (Figure 6) and show no peaks for the TH tetramer of about 15 nm in both the 1:1 and 2:1 TH:MDNPs samples, indicating that all TH must be absorbed by the nanoparticles.

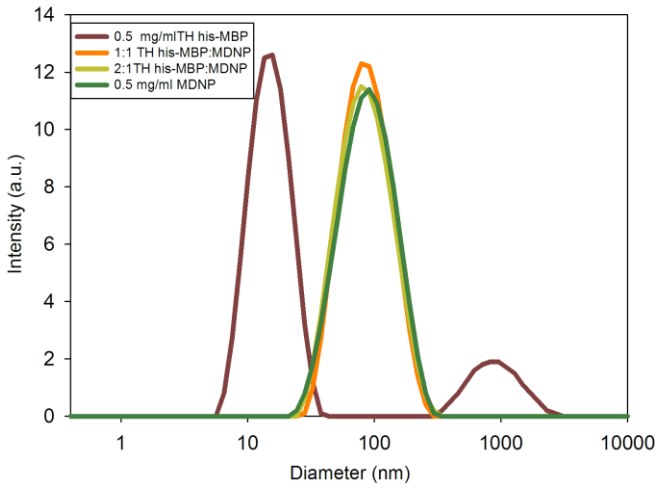

Figure 6: Size distribution of TH-loaded MDNPs. *Intensity-based size distribution was obtained by dynamic light scattering to confirm loading below saturation.*

4.2.2 Loading of TH onto pSiNPs

DLS was used as a primary method to assess loading of TH into pSiNPs. Preliminary loading experiments with different concentration combinations of TH and pSiNPs in 20 mM Hepes, 200 mM NaCl, pH 7.0 buffer, which is the standard buffer used in TH preparations, did not show any sign of TH peaks disappearing from the size distribution plots obtained by DLS (data not shown). In order to achieve loading, other buffers were prepared with lower NaCl concentration (50 mM instead of 200 mM) and lower pH (5.5, 6.0, 6.5 instead of 7.0). The most promising results were obtained with buffers of pH 6.0 and 5.5. Loading at pH 6.0 was compared with pH 7.0 and their respective control samples (Figure 7).

The peak around 15 nm corresponding to tetrameric TH still in solution, is still visible after loading into pSiNPs at pH 7.0 (Figure 7B, orange curve) although it is much lower than free TH at this pH (Figure 7B, brown curve). No free TH was found after loading into pSiNPs at pH 6.0 for the TH loaded into pSiNPs indicating that it could have been absorbed into the pSiNPs. However, for the TH control (Figure 7A, brown curve) no TH peak could be seen either, indicating that TH must have formed aggregates of the same size as the pSiNPs. Loading could thus not be confirmed by DLS as it cannot distinguish between loaded or aggregated TH.

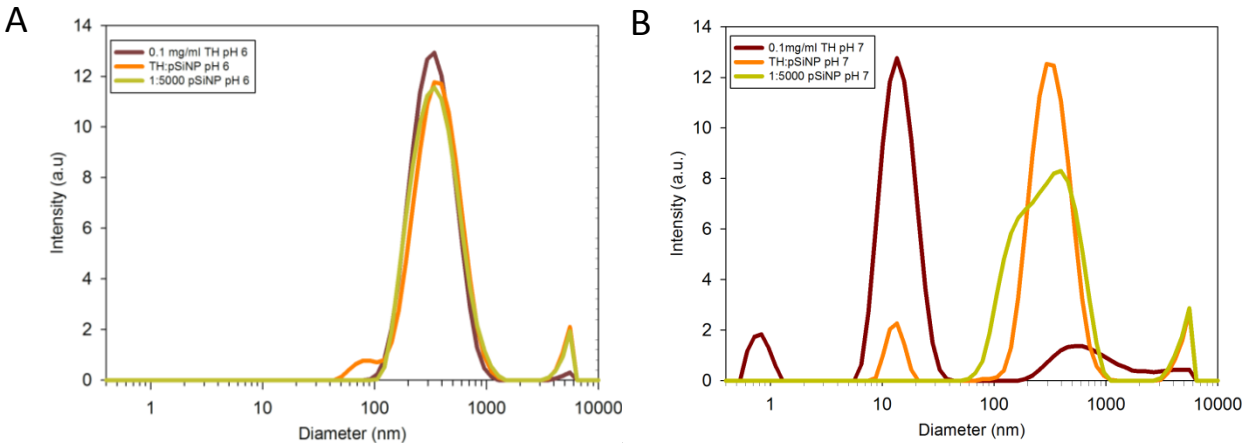

Figure 7: Size distribution of TH loading into pSiNPs based on intensity signals from dynamic light scattering. *A) Size distribution after loading at pH 6.0. B) Size distribution after loading at pH 7.0.*

4.3 Stability of TH-loaded MDNPs

Successful loading of TH into MDNPs led to the investigation of the stability of TH-loaded MDNPs both with regards to incubation at physiologically relevant temperature and to the rate of temperature-dependent denaturation.

4.3.1 Time-dependent stability measurements using DLS

The time-dependent stability of TH-loaded MDNPs was analyzed at 37 °C by monitoring the Z-average diameter obtained from DLS (Figure 8). TH quickly aggregates within 100 min (Figure 8, orange curve), whereas the MDNPs seem to prevent (in the case of 1:1, Figure 8, yellow curve) or delay (in the case of 2:1, Figure 8, green curve) aggregation depending on the TH:MDNPs ratio.

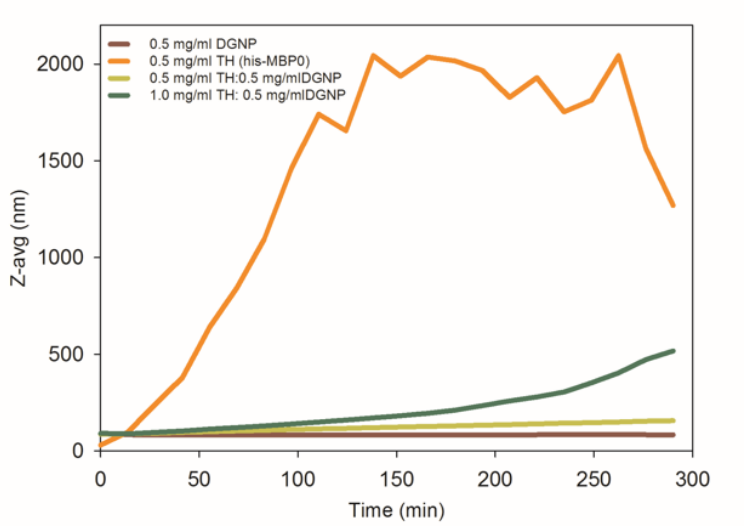

Figure 8: Time-dependent stability of TH-loaded MDNPs at 37 °C. *Each curve is the average of 3 independent experiments.*

4.3.2 Temperature-dependent stability of TH-loaded MDNPs

Stability dependent on temperature in a range of 5 – 60 °C was also monitored by changes in the size measured by DLS (Figure 9). Both the z-average diameter of TH (Figure 9A, orange curve) and the peak 1 intensity diameter of TH (Figure 9B, orange curve) increases from a temperature of 35 °C showing that TH rapidly aggregates from about physiological temperature. None of the two TH-loaded MDNPs show an increase in size before 40 °C and thereby showing that they improve the thermal stability of TH by a few degrees. In addition, we can see that for the 1:1 (w/w) TH:MDNPs the aggregation goes slower as the slope of the curve is less steep (Figure 9A, yellow line; Figure 9B, yellow line).

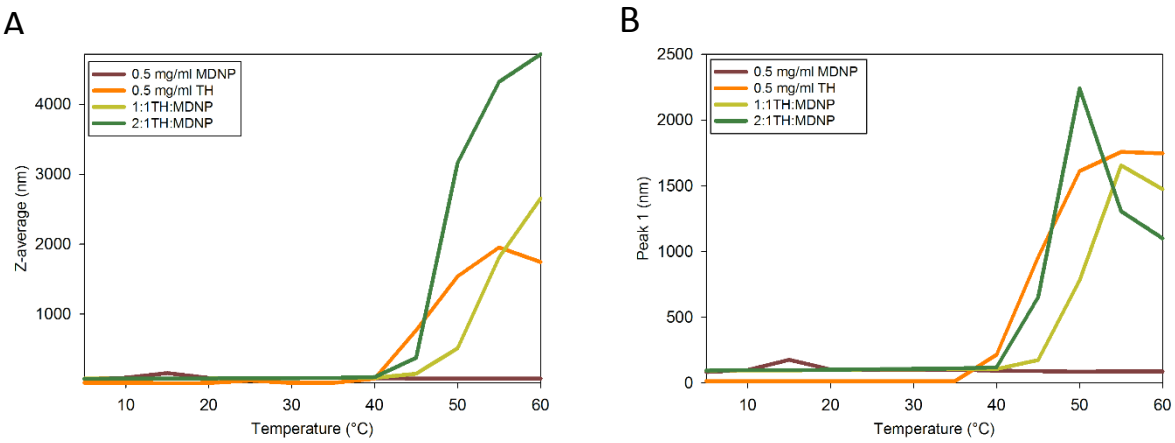

Figure 9: Temperature-dependent stability of the TH-loaded MDNPs*. A) Z-average diameter and B) peak intensity diameter changes upon temperature increase. Each curve is an average of three replicate measurements.*

4.3.3 Th-T assay of TH with pSiNPs

Th-T binding to TH after incubations at pH 6.0 and pH 7.0 for loading into pSiNPs was monitored by fluorescence (Figure 10), to determine if TH aggregated during loading. This could explain what happens to the TH peak that disappears from the size distribution by DLS. The rapid increase in intensity of positive control shows that liposomes induce the formation of soluble aggregates within 300 min (Figure 10, green data points). The intensity of the TH loading into pSiNPs using pH 6 buffer increases quicker when the Th-T assay is also performed in this buffer than when the pH is adjusted before the assay, or loading is performed at pH 7. This confirms the DLS assumption that the reason no free TH was observed is due to aggregation (Figure 10A, yellow and orange data points).

Since no compartment membrane marker, or appropriate staining method to visualize this was found the complex entering the cells could not be confirmed beyond the fact that utilizing the confocal microscopic methods discussed, this remained very likely.

An interesting point, however, is that in the presence of pSiNPs TH aggregates less at pH 6 than when without pSiNPs. This could indicate some sort of protection from aggregation, whereas this effect could not be seen when using pH 7 buffer.

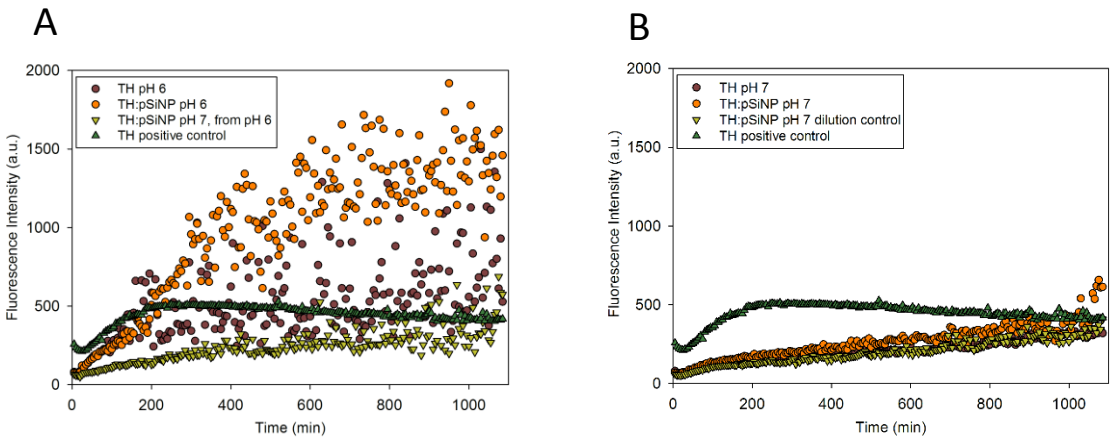

Figure 10: Th-T assay after TH loading in MDNPs at pH 6 and 7. *Th-T binding monitored by fluorescence to determine the formation of soluble aggregates after TH-loading at A) pH 6.0 and B) pH 7.0.*

4.4 Activity measurements

TH activity assays were performed to find out if loading procedures have an effect on the function of TH. The TH reaction was timed and the amount of L-DOPA produced by TH-loaded NPs was measured using HPLC and compared to non-loaded TH both at initial mixing of TH and NPs and after 1.5 h incubation on ice (Figure 11). We can see that MDNPs seem to stimulate TH activity both at the initial time and after 1.5 h (Figure 11A). For pSiNPs, there might be a slight stimulation of TH activity at pH 7 but not at pH 6 (Figure 11B). In general there is a trend in that measuring the same sample after 1.5 h the overall L-DOPA production is less than at the start.

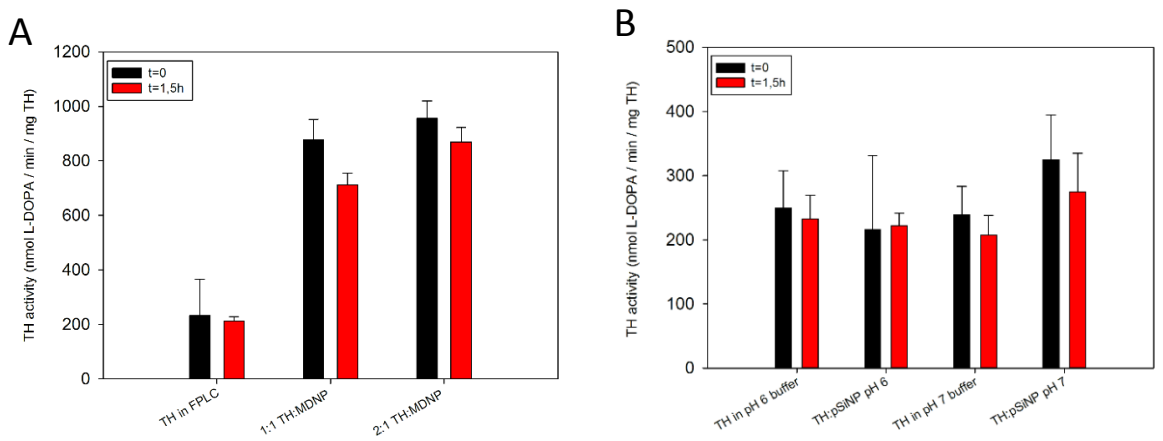

Figure 11: Activity of TH in different nanoparticle preparations. *Assays were performed immediately after preparation of samples, t=0, and after 1.5 h incubation on ice. 9A) Shows activity measurement results of TH:MDNP, and 9B) shows activity results for TH:pSiNP.*

4.5 Fluorescence and confocal microscopy of mouse brain sections

In vivo experiments were performed to see if TH-loaded MDNPs can enter brain cells. These experiments were only performed with MDNPs as they are able to load a considerable amount of TH and seem to stabilize TH thermally and over time. In order to detect the localization of TH-loaded MDNPs within the brain tissue, fluorescent dyes were kindly attached to TH (Alexa568) and nanoparticles (Atto488) by Maria Teresa Bezem and Didier Betbeder, respectively. The dyes were not used simultaneously due to preliminary examination showed that using both dyes at the same time induced aggregation.

4.5.1 Fluorescence microscopy brain maps

Fluorescence images at low magnification were taken using a 2.5x objective of the whole with 50% overlap between each image. In this way, a whole map could be constructed to show the distribution in the brain (Figure 12). None of these sections were stained; instead the system was tuned so that autofluorescence would show the normal tissue, and then using the same settings for each brain map. The section of the mouse brain injected with PBS (Figure 12A) was upside down on the microscope slide and the whole after the injection can therefore be seen at the top left of the brain. The Atto-488-labeled MDNPs (Figure 12B) and Alexa-568 labeled TH-loaded MDNPs (Figure 12C) are located in the area close to injection and do not distribute far into the brain.

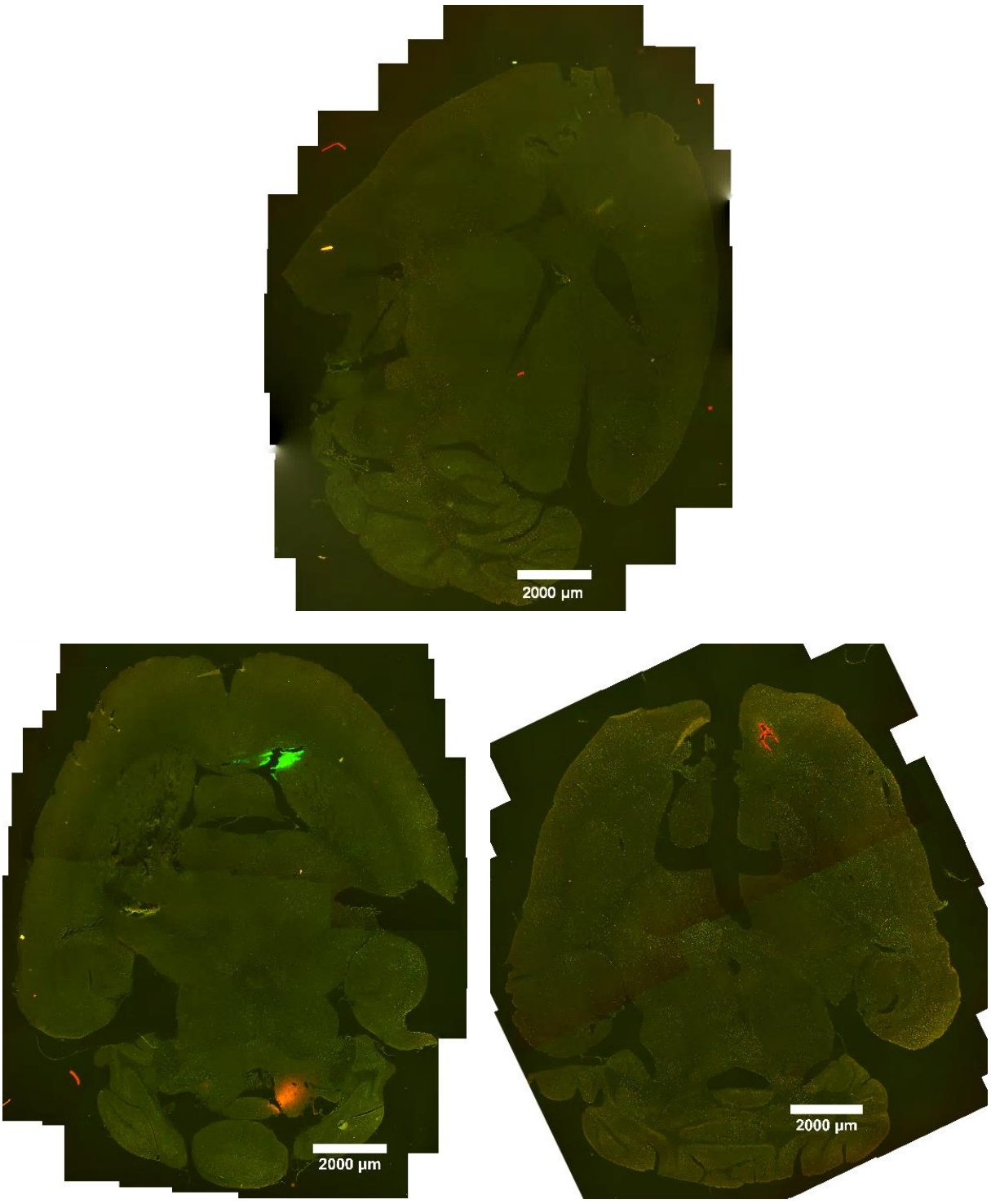

Figure 12: Mouse brain maps of selected section showing injection sites. F*luorescence images taken with 2.5x objective and merged with Photoshop CS4 (Adobe) in order to show complete section maps of mouse brains injected with A) PBS (top), B) Atto-488-labeled MDNPs (bottom left) and C) Alexa-568-labeled TH-loaded MDNPs (bottom right).*

4.5.1 Fluorescent microscopy of injection sites

Sections of mouse brains were imaged using a 20x magnification to determine the local biodistribution of the injected MDNPs (Figure 13). Both the green Atto-488-labeled MDNPs and the red Alexa-568-labeled TH-loaded MDNPs were observed close to the injection site, penetrating the tissue immediately surrounding the injection site.

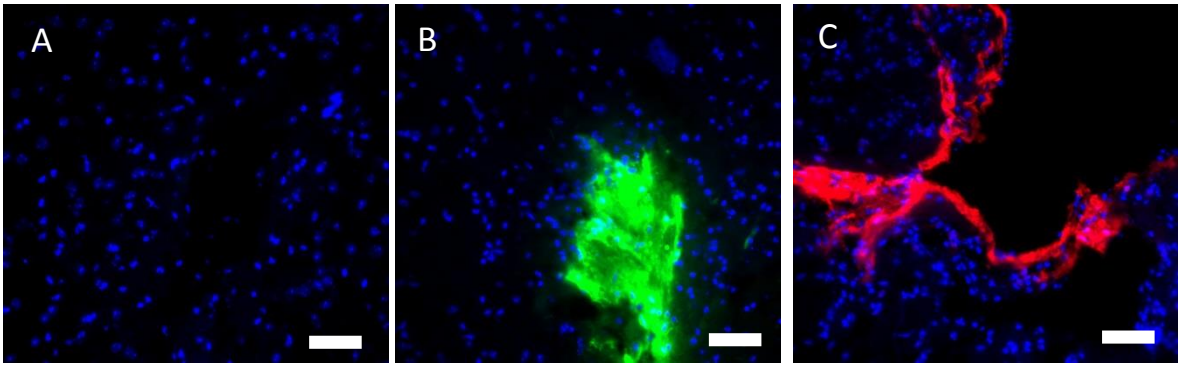

Figure 13: Fluorescence images of the injection sites of mouse brain sections*. Brain section of mice that had been injected with A) PBS, B) Atto-488-labelled MDNPs in green or C) Alexa-468-labelled TH-loaded MDNPs in red were imaged using a 20X objective at their respective injection site. Scalebars are 50 µm and cell nuclei are stained with DAPI shown in blue.*

4.5.4 Confocal imaging of brain sections

Using the Z-stack function of the confocal microscope the section could be examined layer by layer from a top view, examining a single layer at a time. TH-loaded MDNPs can be seen in such a proximity to DAPI stained cell nuclei, that the notion that the TH-loaded MDNPs has entered cells seems feasible (Figure 14). This, however, shows only a single selected stack. Using the entire stack a 3D rendering of the section was made in Fiji (Figure 15). Here the localization of the TH-loaded MDNPs could be clearly seen surrounding the immediate outside of nuclei, once again supporting the notion that they enter cells.

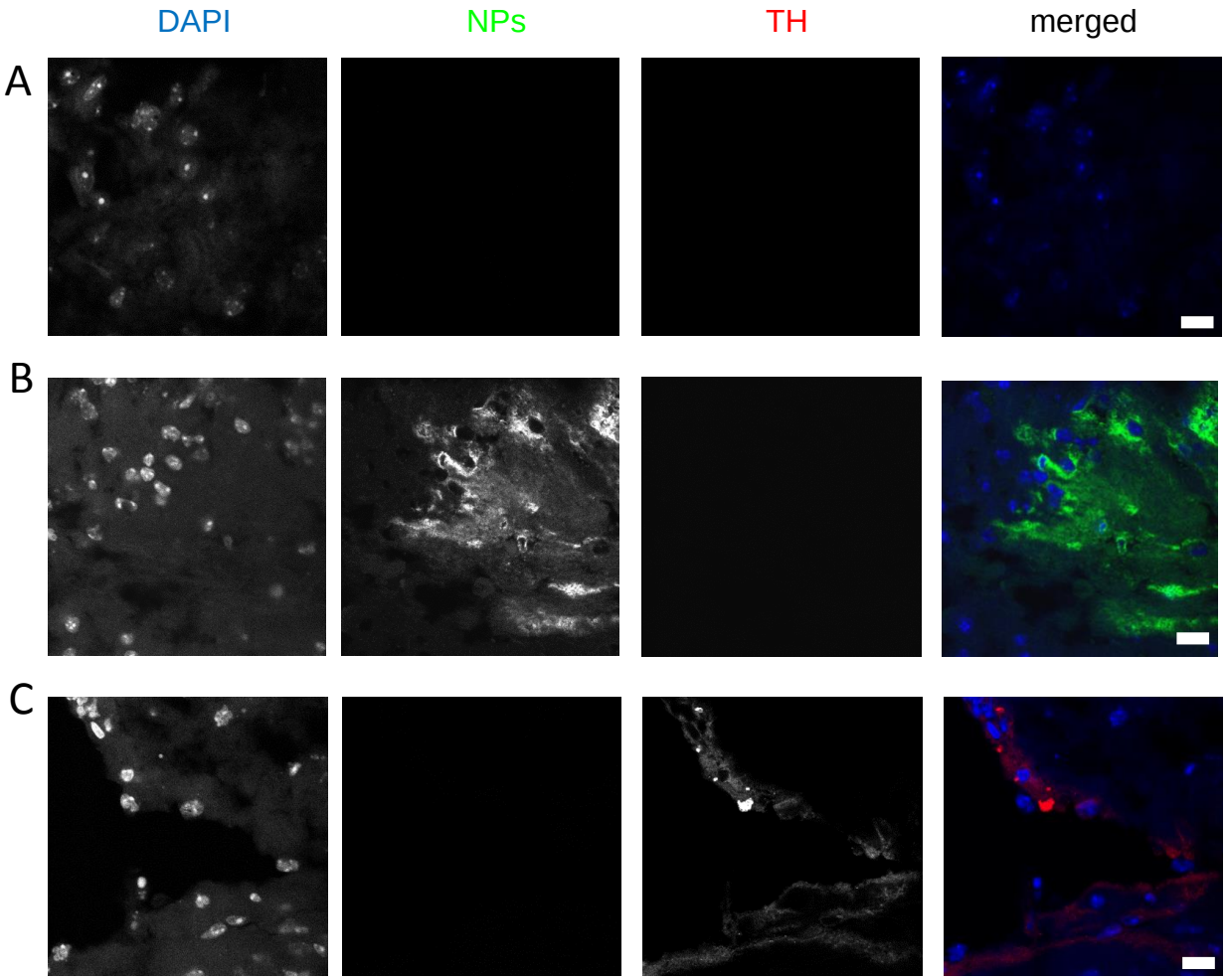

Figure 14: Confocal images of parts of injection sites of mouse brain sections. *Brain section of mice that had been injected with A) PBS, B) Atto-488-labelled MDNPs in green or C) Alexa-468-labelled TH-loaded MDNPs in red were imaged using a 63x objective at their respective injection site. Scalebars are 10 µm and cell nuclei are stained with DAPI, shown in blue.*

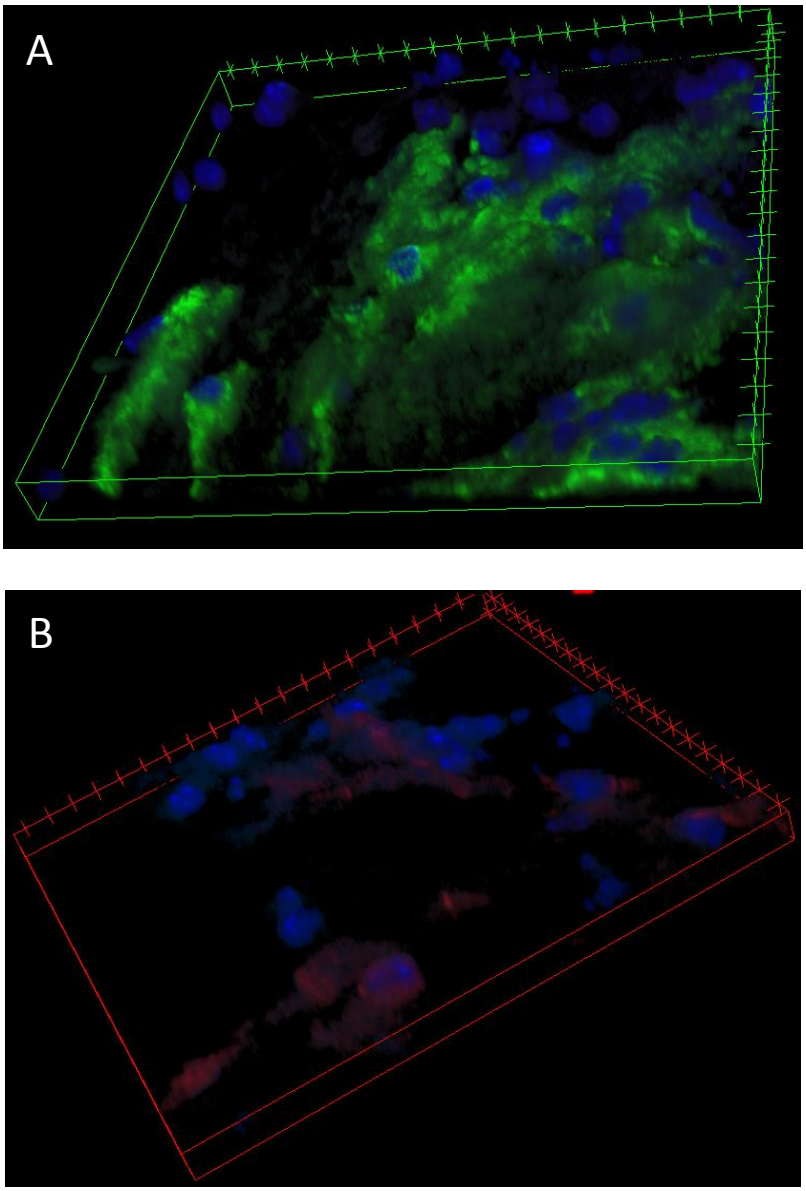

Figure 15: 3D rendering of confocal microscopy Z-stacks of mouse brain sections. *Confocal microscopy was used to obtain a Z-stack, and then the FIJI software was used to make a 3D projection of these images. A) Section showing nuclei of brain tissue cells, stained with DAPI (blue) and Atto 488 linked DGNP+ spread throughout the tissue. B) Nuclei stained with DAPI (blue) and Alexa568-linked TH (red).*

4.5.2 Membrane staining with DiO

In order to gain more information about the potential location of the TH-loaded MDNPs within the brain tissue, the lipophilic marker, DiO, was used to stain the cell membranes of the tissues (Figure 16). Membrane structures were not distinct enough to distinguish

between extracellular matrix and intracellular compartments, leading to the need for another stain to evaluate if TH-loaded MDNPs are entering cells.

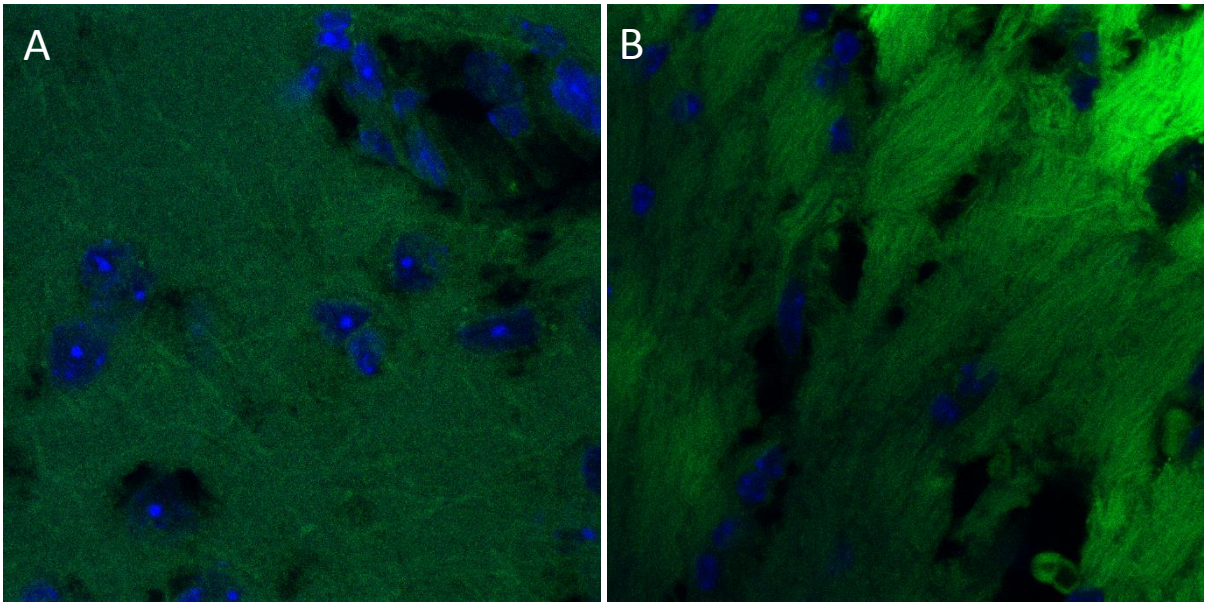

Figure 16: Confocal images of mouse brain sections where membrane was stained with the green fluorescent and lipophilic dye DiO. A) Section stained with 1µM DiO for 5 min and B) with 2µM DiO for 5 min. Cell nuclei are stained with DAPI (blue) and scalebar is 10 µm.

4.5.3 Membrane staining with Wheat Germ Agglutinine (WGA)

An Alexa568 conjugate of WGA (Life Technologies) was used to stain the cell membrane. At the section surface, the staining seemed good, but it only penetrated about 3 µm into the section (Figure 17G). An optimization with different permeabilization procedures were tested on mouse brain sections of a blank control mouse brain and evaluated by confocal microscopy imaging in the YZ-plane that gives a sideview of the section (Figure 11A-D) and compared to sections from the Atto-488-labeled MDNPs injected mouse brain.

In all images it can be seen that the WGA Alexa568 did not completely penetrate the sections, and only 0.5-1 µm deeper penetration was seen due to incubation time and detergent for permeabilization (Figure 17G). Also from 17G it was seen that no permeabilization, m1_is1 and m1_is2 showed that without any permeabilization the WGA penetrated almost as deep into the tissue as with permeabilization with detergents. The WGA follows the topography in the section, penetrating approximately 2,5 to 3 µm into the tissue. In Figure 17 E and F the images were of the injection site of TH:MDNP-Atto488,

showing that the complex is distributed throughout the entire section, as the top of the section is clearly marked with red fluorescence from WGA.

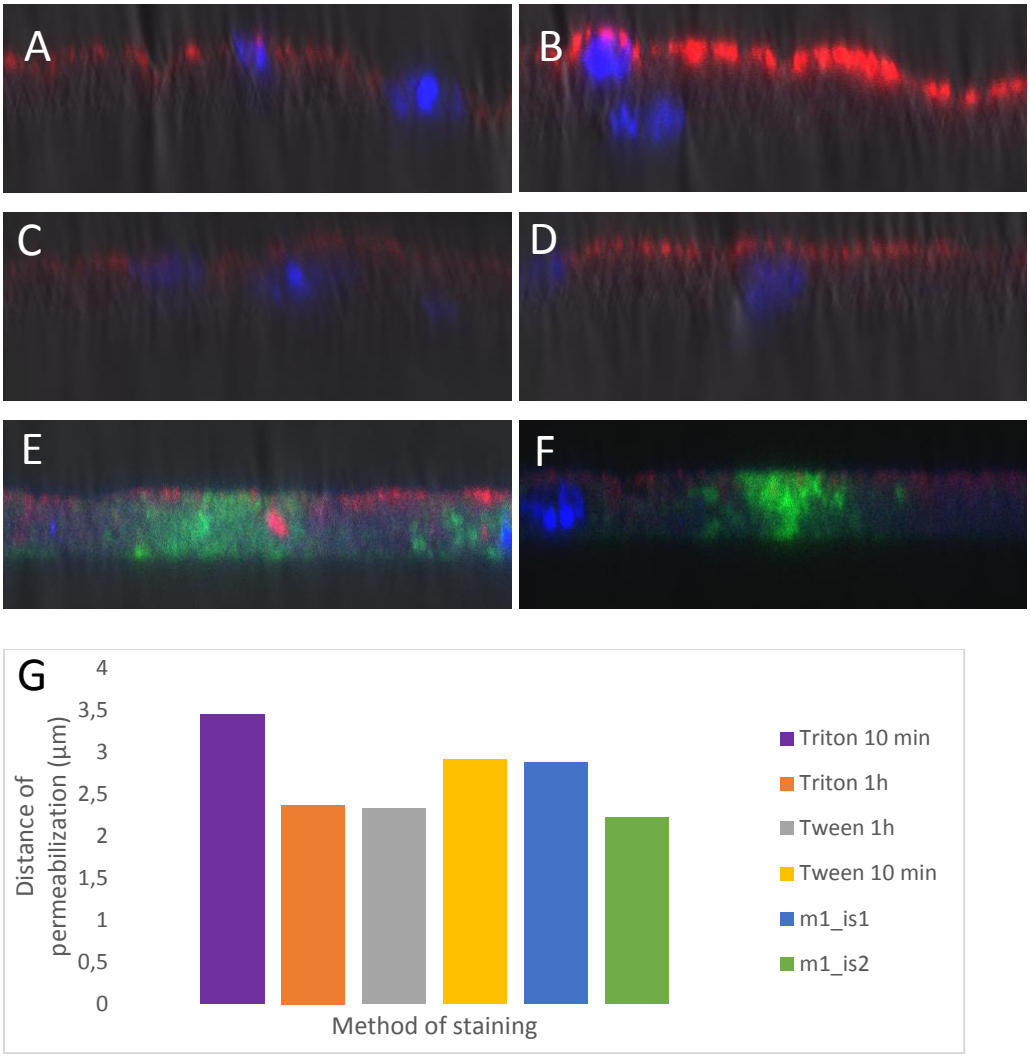

Figure 17: Optimization of cell membrane staining. *A-F) Side view of sections from mouse brain that had been injected with Atto-488 labelled MDNPs in green and stained with Alexa568-labeled WGA in red after treatment with A) Tween for 10 min, B) Triton for 10 min, C) Tween for 1h, D) Triton for 1h or E) and F) without treatment of detergents for enhanced permeabilization were imaged in the yzx-plane using confocal microscopy. Cell nuclei were stained with DAPI shown in blue. G) Average depth of dye penetration using different detergents and washing times before staining, where m1_is1 and m1_is2 signify WGA staining without any permeabilization from two different sections.*

5 Discussion

Controlled protein-drug delivery from nanoparticles is a potential approach for enzyme replacement therapy. The purpose of the present investigation was to develop protein-loaded NPs using MDNPs and pSiNPs loaded with TH, a large protein with large medical interest since it catalyzes de rate-limiting step in the synthesis of dopamine and other catecholamine neurotransmitters. For the NPs to be feasible NCs of TH, the loading with the protein needs to be confirmed. The primary method for confirmation of loading used in this work was DLS, which shows advantages compared with other methods. A reason for this lies in the fact that it is the scattering of the laser off the particles and aggregates in the sample solution, which is does not interfere severely with the samples.

There are examples of other methods used to confirm loading or bioconjugation of some kind onto NPs in the literature, such as AFM [42]. The problem presented with this mode is that the MDNPs have, in previous experiments, not survived the imaging process, as the interaction with the cantilever has disrupted and distorted the particles. Future prospects could be investigating measurements with the non-contact mode of the AFM, hoping that the tapping and contact mode was responsible for the distortion of the MDNPs. For the pSiNPs, however perhaps such a method could be interesting to apply in the future, but since DLS has functioned so well so far for both NPs it was seen as appropriate to use the same method of characterization.

There are also examples protein loading into poly L-lactide-co-glycolidic (PLGA, a biodegradable polymer) based NPs, but loading degree is found with a release study, since the protein is incorporated into the NPs during production [43]. Release studies could be planned for the future, but so far finding loading by titration of proteins and finding the concentrations were all the protein no longer is absorbed has proved sufficient.

In summary the reasons for using the DLS are many: Firstly, DLS quickly shows if total loading has occurred (e.g. all the protein has entered into a complex of some sort with the NP), and eventually, free protein can also be observed in parallel (a ref, to DLS). Secondly, concretely for TH, if no more free TH is present in the sample, then the characteristic peak of

approximately 13-20 nm will disappear, leaving only the peak of approximately 90 nm for MDNPs, or 180 nm for pSiNPs.

5.1 Comparison of MDNPs and pSiNPs as nanocarriers for TH

Part of the interest in the comparison between the MDNPs and the pSiNPs (the two NPs selected in this study) as a NC for TH lies in the fundamental differences between these NPs themselves. The MDNPs consist of organic building blocks, with cross linked maltodextrin making a positively charged NP, with a DPPG core [25]. This makes them fundamentally different from the pSiNPs, which are inorganic, synthesized from silicon wafers through electrochemical etching in HF, and presumably harder [44].

The primary loading experiment showed in Figure 6 illustrates how the DLS method confirms loading since the peak of free TH no longer appears up to 2:1 (TH:NP; w/w) ratio. The fact that the size of the TH:MDNP complex does not change significantly after loading is consistent with the finding of other groups working with loading proteins and/or phospholipids into similar types of MDNPs with a lipid core where the protein attaches [25]. Since both 2:1 and 1:1 w/w loading is possible, the MDNPs already appear as a good candidate to move forward with, so why move forward investigating the pSiNPs?

An advantage of the use of pSiNPs is the highly tunable surface charge, which allows different interactions with drugs or other payloads. However, Shahbazi et al. also found that the surface charge was related to the toxicity of similar pSiNPs, and that hydrophilicity or hydrophobicity also had an effect [45], where negatively charged and hydrophile surfaces gave the least toxic effect in cell experiments. This is in itself a factor that allows tuning of the pSiNPs to avoid unwanted toxic responses. There are also examples from the literature showing that loading of peptides onto pSiNPs has been achieved, usually through some sort of functionalization [46-49]. Furthermore, small molecule drugs, such as methotrexate (an anticancer drug), have also been loaded successfully to porous silicon nanoparticles with positively charged surface, which have been shown to function as a carrier enabling an enhanced dissolution rate of drugs that are otherwise poorly water-soluble [50].

Furthermore the particles can be manipulated to have a specific pore size and surface area which could potentially accommodate several different types of drugs. Porous silicon nanoparticles have been investigated as NCs for different drugs depending on the size of the

particles as well, from nanoparticles to microparticles, for example the loading of Melatonan II, a peptide, onto thermally hydrocarbonized nanoporous silicon microparticles [51]. Thermal hydrocarbonization is a method of coating the surface of pSiNPs with hydrocarbons by exposing the NPs to a 1:1 N_2:acetylene gas flow at 500 °C for 15 min, and is a good example of how the surface of such particles may be specialized for specific payloads.

However, since the foundation of the pSiNPs in a way is the Si-wafer, then the pSiNPs could be expected to be more rigid than the polysaccharide matrix the MDNPs are made up. Thus, despite their stablished potential as NCs in general, a concern could be raised on the specific use of pSiNPs as NPs for TH, since the adsorption of this complex tetrameric enzyme with rigid surfaces could change TH conformation, probably causing denaturation and loss of TH function.

Whereas DLS provided rather conclusive and satisfactory results with respect to the uploading of TH onto MDNPs, and on the functionality of these NCs, our results are not conclusive with respect to the loading for the pSiNPs. One of the issues with this particular nanoparticle was that the loading of the TH onto the NPs was difficult to confirm simply by DLS, since free TH was always visible in the data. Using different pH buffers with different HEPES and NaCl content, 50 mM HEPES buffer pH 6, with 50 mM NaCl, was found to be the best for uploading the enzyme. This buffer consisted of the same buffer components as the fast protein liquid chromatography (FPLC) standard buffer which was normally used for purification, characterization and handling of TH, but with different buffer and salt concentrations and, notably, lower pH (pH 6 vs pH 7 in the FPLC buffer). We used this lower pH buffer, since we hypothesized that lowering pH and NaCl concentration would affect the surface chemistry of the pSiNPs just enough to give a measurable interaction with TH resulting in loading. Finally with this pH 6-buffer no discernable peak for TH could be seen upon incubation with the pSiNP when 0.1 mg/ml TH was incubated with a 1:10000 dilution of the pSiNP sample.

However, we could not disregard that lowering the pH would not only affect the surface of the NPs, but also the enzyme itself, which seemed to quickly aggregate (Figure 7). It has actually been shown that pH 7.0 is optimal for TH activity and stability, as a reduction of pH leads to release of the non-heme active site iron and reduced activity and stability [52]. Actually 50% of iron is released upon a pH decrease from 7.0 to 6.0 [52]. This may

explain the propensity we encountered to TH aggregation at pH 6, explaining the disappearance of the TH peak. A weakness with using DLS for this particular experiment was that the sample containing only TH would create aggregates which the DLS measured to have approximately the same diameter size as the pSiNPs.

Another flaw with this method when looking into the size of pSiNPs is the fact that in the DLS method the assumption is that the particles examined are hard spheres. This, of course, is not the case when looking into the pSiNPs. The method of synthesis itself does not make a spherical shape of pSiNPs feasible [44], the pores are made in a single direction, and then the Si-wafer is shattered by ultrasonication. As a comparison, the MDNPs are spherical [53] and the method is therefore more suited for determining their size. pSiNPs not being spherical could be interpreted to mean that the polydispersity of the sample might be interpreted by the DLS software to be larger, and their shape also makes stacking of pSiNPs possible, and is a weakness of the method that needs to be taken into account.

Thus, the DLS method could be used to confirm loading for MDNPs, but not conclusively for pSiNPs. In order to verify or debunk loading and investigate the degree of TH aggregation, a ThT fluorescence assay was performed. The increase of measured ThT fluorescence is linked to formation of amorphous or amyloid aggregates through cross-β intermolecular aggregation [36]. We observed that preparing TH:pSiNP in 50 mM HEPES buffer, pH 6, with 50 mM NaCl buffer and then increasing the pH to 7 as well as only TH in the pH 7 buffer aggregated at the same pace. Samples kept in the pH 6 buffer aggregated much faster, only initially beaten by the positive control into which liposomes were added to promote aggregation (Baumann et al., in preparation). All three results are seen in Figure 10, and provide interesting information pertaining to the TH:pSiNP complex. What we already knew was that after adjusting the pH after 1,5 hours of incubation the DLS gave no peak for free TH. Now this knowledge could be paired with the fact that this sample aggregates at the same pace as samples kept in the pH 7 buffer in which it was more stable (Figure 7). This could be seen as an argument for loading since we can assume that no free TH peak could be detected in the sample in DLS at this point at the same time as the aggregation would be the same as the pH 7 samples. This assumption could only be correct if the pSiNPs themselves do not interfere with the cross-β intermolecular aggregation at some level. Since no hindering effects are observed comparing the TH:pSiNP pH 7 and TH pH 7 samples, the

pSiNPs interfering in fibril formation is less likely [54]. So does the pH change have an effect on stability of TH in TH:pSiNP? The essential goal with the pH alteration was that we were hoping loading would occur through some sort of diffusion at a slightly lowered pH, and then an increased pH would either show release of TH or no release. Since the DLS data showed no release (Figure 7), then the hope for the pH altered complex was that the TH was affiliated with the NP in some fashion. Since the TH:pSiNP kept in pH 6 buffer throughout the ThT assay aggregated at a much higher rate than the complex where the pH was readjusted this could be taken as an argument that loading had taken place.

Since loading seemed so much more straightforward for MDNPs, these were chosen for further stability studies using DLS. Figure 8 shows the Z-average diameter of the TH:MDNP complex over time at 37 °C. When the pure TH sample aggregated quickly, wih a Z-average rapidly increasing from approximately 20 nm to the 2000 nm range. After a while the Z-average starts to decrease, indicating precipitation of much larger particles. While the protein alone aggregates relatively quickly, Figure 8 also shows that once in a complex with MDNPs, the complex does not aggregate at a 1:1 w/w ratio, and also delays the aggregation of 2:1 w/w ratio complexes, revealing an effective stabilization of TH when bound to MDNPs. Although these results indicate that the more TH is loaded onto the MDNPs, the less the MDNPs will protect TH from aggregation, it is important to note that the complex remained stable at 37 °C for over 250 min. The implication, of course, is that such a complex would in theory remain stable in a in vivo situation, which in turn would be preferred should the TH:MDNP in the future be used as a nanoreactor/nanocarrier in an ERT.

Time dependent stability measurements had proven favorable for the TH:MDNPs, therefore the stability and aggregation of the TH:MDNP complex was studied as the temperature was changed. Using DLS, the Z-average particle size and largest peak maxima were measured over a range from 5 to 60 °C. What was once again seen was consistent with the previous stability experiment for TH:MDNP. The Peak 1 value started increasing between the 35 and 40 °C step, earlier than the other samples with MDNPs, and the Z-avg increased faster for TH than for the TH:MDNPs. Once again a somewhat protective function of the MDNPs was found, but this effect would not stabilize the TH:MDNP complex for much higher temperatures. Once the temperature was high enough (over 40 °C (see Figure 9)), all the complexes aggregated as well. When looking at this from a perspective of potential medical

use, such temperatures would not be feasible unless the patient was suffering from a fever. This means, however, that there are some potential limitations to how the complex might be used.

It was mentioned earlier that due to the very nature of both NPs used in this study, their interaction with TH would be very different. Should loading take place, and any conformational change happen this would be more likely to affect the protein instead of the NP in the case of the rigid inorganic pSiNPs. To find out if being in the complexes affected the potential TH function, their activity was measured (Figure 11). The first thing that became clear from this experiment was that the TH:MDNP complex in FPLC buffer had the highest activity, nearly 1000 nmol L-DOPA/min/mg TH. None of the other samples came close to these numbers, so what does this mean? Since the activity is higher than in the blank with only TH in FPLC buffer would be tempting to assume that the difference observed is due to the fact that the activity increases once incorporated into MDNPs.

A more reasonable explanation, perhaps, would be to assume that the stabilizing effect that the MDNPs have towards the TH came into play. For the experiment, a stock of sample was prepared, and immediately the activity was measured. After 1.5 hours, the same time period found to remove free TH peaks in the DLS for TH:pSiNPs, all samples were measured again. A trend was apparent from looking at the data in Figure 11, for every sample measured at t=0 had higher measured activity than at t=1.5 h. This could be seen as an argument for MDNPs protecting the activity of TH, and since TH was not taken directly from the tank, thawed and pipetted into the samples, but instead was thawed, diluted and had its concentration measured first. This process took a few hours, but since the enzyme in the sample with TH alone and with TH:MDNP complex came from the same stock, it could also be stated that the TH in FPLC sample should have the highest possible activity for these samples. So what can be the reasons for these peaks?

Perhaps the answer lies in the TH batch itself. The SDS PAGE analysis of the degree of purification of the enzyme (Figure 5) showed that there was still some faint traces of MBP, the fusion partner used under purification) in the protein samples used for these experiments, but this does not provide a clear explanation for the difference in activity. What we were able to discern from this, however, was that the TH:MDNP complex of both 1:1 w/w and 2:1 w/w had a beneficial effect on the activity.

The samples from the pSiNP all had activity, which is important for a number of reasons. Firstly, the blanks all had zero L-DOPA production, both samples without any TH at all and the blanks where TH is not added until after the addition of stop solution. The fact that any peak for L-DOPA was present at all is proof that TH has activity in the TH:pSiNP complex. If the TH:MDNP having some protective effect on TH in terms of activity could be said, then from Figure 11 the same conclusion could be reached, albeit not as strongly. A problem with these results were that there was not much difference between TH only samples and TH:pSiNPs, so that the only thing that could be said for sure was that for these samples activity of TH was retained, even in the complex with pSiNPs. These results indicate that in addition to TH aggregation, which is expected to strongly decrease TH activit, some TH is still attached to TH in a functional manner.

5.2 The distribution of TH-loaded MDNPs in brain

In vivo experiments were also conducted, and due to the results discussed previously only TH:MDNP was used for this. This was due to several reasons, being the previous cell experiments performed by the group (Bezem et al., in revision) and the fact that the TH:pSiNPs had not proven as promising as we had hoped. The reasoning behind performing a primary experiment with stereotaxic surgery and injecting the NPs directly into the brain was manifold. This way the TH:MDNPs were exposed to brain cells in an *in vivo* situation without having to penetrate the BBB, or being exposed to first pass effect [55]. Comparison of our two NPs as TH-carriers had already proven a clear favorite for ERT, but in order to be used for this purpose the complex needed to be taken up by the cells in the brain in an in vivo situation. Going through the fluorescence microscopy data should help prove this was the case for the TH:MDNPs complex.

The experiment was performed as described in the procedures section, and Figure 12 shows the first fluorescence microscopy image of the brain sections. Bleed-through, the simultaneous excitation and detection of signal from two or more fluorescent dyes showing the signal of two channels in a single channel, was not an issue for these experiments due to the fact that when the complex was injected only the protein or the NP was labelled. Another point to support this was the difference in excitation and emission wavelengths of the fluorophores chosen. The choice to not have both TH and NPs marked at the same time

was due to examination in the DLS showing aggregations once both fluorescent labels were present. In the Figure 12 the brain maps are presented. They should as such only be seen as a representation of the brain as a whole, whilst the accuracy of the image contains some errors. This was due to the software used for the merging in some areas erred, and the fact that each of these images are built up of approximately 70 fluorescence microscopy images each. These images show how the fluorescent markers are detected in the tissue close to the injection site

Figure 13 also illustrates the injection sites located in the tissue, but in this figure the nuclei of the cells had been stained with DAPI. The images show the injection site of the brain, and speaks a strong case for the TH:MDNPs being distributed within the tissue itself. A limitation with fluorescence microscopy is that the resulting image shows a projection of fluorescence of every plane summed up into one, since out of focus fluorescence also contributes to the detected signal, as mentioned previously. This meant that fluorescence microscopy was a very good first indicator, but could not be used exclusively to prove that TH:MDNP entered the cells *in vivo*.

In order to more clearly visualize the section layer by layer to analyze where the TH:MDNPs could be found was done using confocal microscopy. Use of confocal microscopy to analyze tissue sections is described in several papers [56-58].

Figure 16 shows the first attempt at membrane staining using the DiO dye. The results did not show clear membranes in the section, due in part to very low fluorescence. For the images taken of these dyed sections a fear was that what was observed was only autofluorescence resulting naturally from having a high laser intensity whilst imaging. It was also possible that the Prolong Gold with DAPI interfered with lipophilic marker DiO.

Therefore, an alternative membrane marker, WGA with an Alexa 568 dye was tested. The motivation for using this lectin, a carbohydrate binding protein, WGA was that this has previously been used to bind membranes and extracellular matrixes [59]. The result, which can be seen in Figure 17 shows Y-sections of the brain sections. Although several permeabilization methods were attempted, the dye never penetrated much farther than 3,5 µm into the section. This did, however prove beneficiary when the staining was performed on sections with TH:MDNP-Atto488, like in Figure 17 E) and F). Here, as in the other

instances, the WGA makes a red line along the top of the section, whilst the green fluorescence from the NPs and blue fluorescence from the nuclei are found below. This was a strong argument for the complex being distributed within the tissue close to the injection site, and also that it could enter cells here.

This notion was supported further by what was found using no membrane marker, but DAPI and taking Z-stacks in a confocal microscope of the brain sections. Figure 14 and 15 show this. Figure 14 shows confocal images of a single plane within the section. Here, A is a section with TH:MDNP-Atto488, B were injected with TH-Alexa568:MDNP, and C was a blank injected only with PBS and stained with DAPI, which is why no green or red fluorescence was detected. In these images it can be seen that the TH:MDNP complexes conclusively are found to be distributed throughout the tissue, and surrounding the nuclei. Another strong arguments for the TH:MDNPs actually entering the cells are the 3D rendering of Z-stacks with the same samples (Figure 15). Here it was clearly demonstrated that the TH:MDNP complexes surrounded the nuclei to such an extent that the complexes having actually entered the cells is very feasible. Since no compartment membrane marker, or appropriate staining method to visualize this was found the complex entering the cells could not be confirmed beyond the fact that utilizing the confocal microscopic methods discussed, this remained very likely.

6 Conclusions

Our results show that the TH:MDNP complexes allow loading of relatively large amounts of TH quickly and efficiently. Furthermore, the complex proved stable over time, and the MDNPs prevented aggregation to some degree over larger temperature ranges. On the other hand loading TH into the TH:pSiNPs proved more difficult. Loading could possibly occur, but was not confirmed.

Based on the stability experiments as well as experiments carried out earlier (Bezem et. al., in revision) the TH:MDNP was used for *in vivo* experiments. Fluorescent markers attached to the TH and MDNPs both appeared in roughly the same area, the tissue surrounding the injection sites. For the TH:MDNP to be a feasible candidate for further development into an ERT, the complex had to enter the cells. Using confocal microscopy, and creation of 3D projections of the obtained images showed that the likelihood of the TH:MDNPs entering the cells was very high. However, until an appropriate method for staining the membranes is found so that internalization can be properly visualized this cannot be confirmed beyond the methods that have been discussed.

7 Future perspectives

There are definitely several paths forward for this project. Through our experiments a proof-of-concept of TH:MDNP was obtained, but in order to reach the goal of use in treatment as an ERT some refinement of the method is needed. Examples of this could be functionalization of the NPs in a way that allows receptor mediated targeting [60]. The potential of this could for instance be to develop a targeting function to pass the BBB, so that intravenous injection is the method of administration instead of direct injection into the brain.

As well as functionalization of the NPs, other studies are needed as well. A toxicity study comparing the two types of NPs should be performed, and there are already plans for xCELLigence assays to be carried out. Furthermore, if the pSiNPs should be used in the future, the some kind of concentration of these nanoaprticles should be found. Hopefully the use of the qNano, an instrument that allows measurements of properties for single NPs as well as determining the concentration of NPs in a solution, will be used to this respect.

8 References

1. Wong, P.C., et al., *Chapter 45 - Motor Neuron Diseases*, in *Basic Neurochemistry (Eighth Edition)*, S.T.B.J.S.W.A.L. Price, Editor. 2012, Academic Press: New York. p. 801-814.
2. Brundin, P., G. Atkin, and J.T. Lamberts, *Basic science breaks through: New therapeutic advances in Parkinson's disease.* Mov Disord, 2015. **30**(11): p. 1521-7.
3. Korner, G., et al., *Brain catecholamine depletion and motor impairment in a Th knock-in mouse with type B tyrosine hydroxylase deficiency.* Brain, 2015. **138**(Pt 10): p. 2948-63.
4. Tristan-Noguero, A., et al., *Study of a fetal brain affected by a severe form of tyrosine hydroxylase deficiency, a rare cause of early parkinsonism.* Metab Brain Dis, 2016. **31**(3): p. 705-9.
5. Siow, Y.L. and K. Dakshinamurti, *Neuronal dopa decarboxylase.* Ann N Y Acad Sci, 1990. **585**: p. 173-88.
6. Nagatsu, T., M. Levitt, and S. Udenfriend, *Tyrosine Hydroxylase The Initial Step in Norepinephrine Biosynthesis* The Journal of Biological Chemistry, 1964. **239**(9).
7. Goridis, C. and H. Rohrer, *Specification of catecholaminergic and serotonergic neurons.* Nature Reviews Neuroscience, 2002. **3**(7): p. 531-541.
8. Gnegy, M.E., *Chapter 14 - Catecholamines*, in *Basic Neurochemistry (Eighth Edition)*, G.J.S. Scott T. Brady, R. Wayne Albers, Donald L. Price, Editor. 2012, Academic Press: New York. p. 283-299.
9. Chen, L. and X. Zhuang, *Transgenic mouse models of dopamine deficiency.* Ann Neurol, 2003. **54 Suppl 6**: p. S91-102.
10. O'Malley, K.L., et al., *Isolation and characterization of the human tyrosine hydroxylase gene: identification of 5' alternative splice sites responsible for multiple mRNAs.* Biochemistry, 1987. **26**(22): p. 6910-4.
11. Lewis, D., D. Melchitzky, and J. Haycock, - *Four isoforms of tyrosine hydroxylase are expressed in human brain.* Neuroscience, 1993. **54**(2): p. 477-92.
12. Haycock, J.W., *Four forms of tyrosine hydroxylase are present in human adrenal medulla.* J Neurochem, 1991. **56**(6): p. 2139-42.
13. Tekin, I., et al., *Complex molecular regulation of tyrosine hydroxylase.* J Neural Transm, 2014. **121**(12): p. 1451-81.

14. Higgins, C.A., et al., *Expression and purification of recombinant human tyrosine hydroxylase as a fusion protein in Escherichia coli.* Protein Expr Purif, 2012. **84**(2): p. 219-23.
15. Hauser, R.A., *Levodopa: past, present, and future.* Eur Neurol, 2009. **62**(1): p. 1-8.
16. Bastide, M.F., et al., *Pathophysiology of L-dopa-induced motor and non-motor complications in Parkinson's disease.* Prog Neurobiol, 2015. **132**: p. 96-168.
17. Visanji, N.P., et al., *Dopamine D3 receptor stimulation underlies the development of L-DOPA-induced dyskinesia in animal models of Parkinson's disease.* Neurobiol Dis, 2009. **35**(2): p. 184-92.
18. Brooks, D.J., *Dopamine agonists: their role in the treatment of Parkinson's disease.* J Neurol Neurosurg Psychiatry 2000, 2000. **68**: p. 685–690.
19. Moldovan, A.S., et al., *The treatment of Parkinson's disease with deep brain stimulation: current issues.* Neural Regen Res, 2015. **10**(7): p. 1018-22.
20. Li, W., S. Chen, and J.Y. Li, *Human induced pluripotent stem cells in Parkinson's disease: A novel cell source of cell therapy and disease modeling.* Prog Neurobiol, 2015.
21. Palfi, S., et al., *Long-term safety and tolerability of ProSavin, a lentiviral vector-based gene therapy for Parkinson's disease: a dose escalation, open-label, phase 1/2 trial.* The Lancet, 2014. **383**(9923): p. 1138-1146.
22. O'Connor, D.M. and N.M. Boulis, *Gene therapy for neurodegenerative diseases.* Trends Mol Med, 2015. **21**(8): p. 504-12.
23. Hemsley, K.M. and J.J. Hopwood, *Delivery of recombinant proteins via the cerebrospinal fluid as a therapy option for neurodegenerative lysosomal storage diseases.* Int J Clin Pharmacol Ther, 2009. **47 Suppl 1**: p. S118-23.
24. Eckhardt, M., *Pathology and current treatment of neurodegenerative sphingolipidoses.* Neuromolecular Med, 2010. **12**(4): p. 362-82.
25. Paillard, A., et al., *Positively-charged, porous, polysaccharide nanoparticles loaded with anionic molecules behave as 'stealth' cationic nanocarriers.* Pharm Res, 2010. **27**(1): p. 126-33.
26. Jallouli, Y., et al., *Influence of surface charge and inner composition of porous nanoparticles to cross blood-brain barrier in vitro.* Int J Pharm, 2007. **344**(1-2): p. 103-9.
27. Qin, Z.T., et al., *Size Control of Porous Silicon Nanoparticles by Electrochemical Perforation Etching.* Particle & Particle Systems Characterization, 2014. **31**(2): p. 252-256.
28. Orosco, M.M., C. Pacholski, and M.J. Sailor, *Real-time monitoring of enzyme activity in a mesoporous silicon double layer.* Nat Nanotechnol, 2009. **4**(4): p. 255-8.
29. Park, J.-H., et al., *Biodegradable luminescent porous silicon nanoparticles for in vivo applications.* Nature Materials, 2009. **8**.

30. Li, Y., V. Lubchenko, and P.G. Vekilov, *The use of dynamic light scattering and brownian microscopy to characterize protein aggregation.* Rev Sci Instrum, 2011. **82**(5): p. 053106.
31. Lorber, B., et al., *Protein analysis by dynamic light scattering: methods and techniques for students.* Biochem Mol Biol Educ, 2012. **40**(6): p. 372-82.
32. Combs, C.A., *Fluorescence microscopy: a concise guide to current imaging methods.* Curr Protoc Neurosci, 2010. **Chapter 2**: p. Unit2 1.
33. Jonkman, J. and C.M. Brown, *Any Way You Slice It-A Comparison of Confocal Microscopy Techniques.* J Biomol Tech, 2015. **26**(2): p. 54-65.
34. Brown, C.M., *Fluorescence microscopy--avoiding the pitfalls.* J Cell Sci, 2007. **120**(Pt 10): p. 1703-5.
35. Khurana, R., et al., *Mechanism of thioflavin T binding to amyloid fibrils.* J Struct Biol, 2005. **151**(3): p. 229-38.
36. Hole, M., et al., *Discovery of compounds that protect tyrosine hydroxylase activity through different mechanisms.* Biochim Biophys Acta, 2015. **1854**(9): p. 1078-89.
37. Kawahata, I., et al., *Accumulation of phosphorylated tyrosine hydroxylase into insoluble protein aggregates by inhibition of an ubiquitin-proteasome system in PC12D cells.* J Neural Transm (Vienna), 2009. **116**(12): p. 1571-8.
38. Wahab, M.F., et al., *Sampling frequency, response times and embedded signal filtration in fast, high efficiency liquid chromatography: A tutorial.* Anal Chim Acta, 2016. **907**: p. 31-44.
39. Son, A.I., K. Sokolowski, and R. Zhou, *Cryosectioning.* Methods Mol Biol, 2013. **1018**: p. 301-11.
40. Pinskiy, V., et al., *A low-cost technique to cryo-protect and freeze rodent brains, precisely aligned to stereotaxic coordinates for whole-brain cryosectioning.* J Neurosci Methods, 2013. **218**(2): p. 206-13.
41. Puigdellivol-Sanchez, A., et al., *Cryostat Slice Irregularities May Introduce Bias in Tissue Thickness Estimation: Relevance for Cell Counting Methods.* Microsc Microanal, 2015. **21**(4): p. 893-901.
42. Tessmer, I., et al., *Investigating bioconjugation by atomic force microscopy.* J Nanobiotechnology, 2013. **11**: p. 25.
43. Mukherjee, B., et al., *Preparation, characterization and in-vitro evaluation of sustained release protein-loaded nanoparticles based on biodegradable polymers.* Int J Nanomedicine, 2008. **3**(4): p. 487-96.
44. Park, J.H., et al., *Biodegradable luminescent porous silicon nanoparticles for in vivo applications.* Nat Mater, 2009. **8**(4): p. 331-6.

45. Shahbazi, M.A., et al., *The mechanisms of surface chemistry effects of mesoporous silicon nanoparticles on immunotoxicity and biocompatibility.* Biomaterials, 2013. **34**(31): p. 7776-89.
46. Ferreira, M.P., et al., *In vitro and in vivo assessment of heart-homing porous silicon nanoparticles.* Biomaterials, 2016. **94**: p. 93-104.
47. Araujo, F., et al., *Microfluidic Assembly of a Multifunctional Tailorable Composite System Designed for Site Specific Combined Oral Delivery of Peptide Drugs.* ACS Nano, 2015. **9**(8): p. 8291-302.
48. Wang, C.F., et al., *Multifunctional porous silicon nanoparticles for cancer theranostics.* Biomaterials, 2015. **48**: p. 108-18.
49. Kaasalainen, M., et al., *Electrostatic interaction on loading of therapeutic peptide GLP-1 into porous silicon nanoparticles.* Langmuir, 2015. **31**(5): p. 1722-9.
50. Wang, C.F., et al., *Dual-drug delivery by porous silicon nanoparticles for improved cellular uptake, sustained release, and combination therapy.* Acta Biomater, 2015. **16**: p. 206-14.
51. Kilpelainen, M., et al., *Nanostructured porous silicon microparticles enable sustained peptide (Melanotan II) delivery.* Eur J Pharm Biopharm, 2011. **77**(1): p. 20-5.
52. Haavik, J., et al., *Recombinant human tyrosine hydroxylase isozymes. Reconstitution with iron and inhibitory effect of other metal ions.* Eur J Biochem, 1991. **199**(2): p. 371-8.
53. Major, M., et al., *Characterization and phase behaviour of phospholipid bilayers adsorbed on spherical polysaccharidic nanoparticles.* Biochim Biophys Acta, 1997. **1327**(1): p. 32-40.
54. Colvin, V.L. and K.M. Kulinowski, *Nanoparticles as catalysts for protein fibrillation.* Proc Natl Acad Sci U S A, 2007. **104**(21): p. 8679-80.
55. Pond, S.M. and T.N. Tozer, *First-pass elimination. Basic concepts and clinical consequences.* Clin Pharmacokinet, 1984. **9**(1): p. 1-25.
56. Aniszewska, A., et al., *The expression of interleukin-6 and its receptor in various brain regions and their roles in exploratory behavior and stress responses.* J Neuroimmunol, 2015. **284**: p. 1-9.
57. Wang, Z., et al., *Polymeric Nanovehicle Regulated Spatiotemporal Real-Time Imaging of the Differentiation Dynamics of Transplanted Neural Stem Cells after Traumatic Brain Injury.* ACS Nano, 2015.
58. Zane, A., et al., *Uptake of bright fluorophore core-silica shell nanoparticles by biological systems.* Int J Nanomedicine, 2015. **10**: p. 1547-67.
59. Baddeley, D., et al., *4D super-resolution microscopy with conventional fluorophores and single wavelength excitation in optically thick cells and tissues.* PLoS One, 2011. **6**(5): p. e20645.

60. Wang, X., et al., *The development of site-specific drug delivery nanocarriers based on receptor mediation.* J Control Release, 2014. **193**: p. 139-53.